lished); Jeffrey Martin Weiss, 1972 (unpublished); and Gordon Bennett Thomson, 1972 (unpublished).
[5]G. E. Gladding, J. J. Russell, M. J. Tannenbaum, J. M. Weiss, and G. B. Thomson, preceding paper, Phys. Rev. D 8, 3721 (1973).
[6]H. H. Bingham *et al.*, Phys. Lett. 41B, 635 (1972); G. Bacci *et al.*, *ibid.* 38B, 551 (1972); G. Barbarino *et al.*, Nuovo Cimento Lett. 3, 689 (1972).
[7]C. E. DeTar *et al.*, Phys. Rev. Lett. 26, 675 (1971); J. M. Wang and L. L. Wang, *ibid.* 26, 1287 (1971); S. D. Ellis and A. I. Sanda, Phys. Lett. 41B, 87 (1972).
[8]E. Leader and M. R. Pennington, Phys. Rev. Lett. 27, 1325 (1971); A. D. Krisch, *ibid.* 19, 1149 (1967); E. Leader and M. R. Pennington, Phys. Rev. D 7, 2668 (1973).
[9]W. E. Ellis, R. R. Kinsey, T. W. Morris, R. S. Panvini, and F. Turkot, Phys. Lett. 32B, 641 (1970).
[10]J. Allaby *et al.*, CERN Report No. CERN-70-12 (unpublished); M. A. Abolins *et al.*, Phys. Rev. Lett. 25, 126 (1970); E. W. Anderson *et al.*, *ibid.* 19, 198 (1967).
[11]R. C. Hwa, Phys. Rev. Lett. 26, 1143 (1971).

PHYSICAL REVIEW D VOLUME 8, NUMBER 11 1 DECEMBER 1973

Study of the η' Meson from the Reaction $K^-p \to \Lambda\eta'$ at 2.18 GeV/c *

Jerome S. Danburg,† George R. Kalbfleisch, Samuel R. Borenstein,‡
Richard C. Strand, and Vance VanderBurg
Brookhaven National Laboratory, Upton, New York 11973

J. W. Chapman, Richard K. Kiang,§ and J. Lys‖
University of Michigan, Ann Arbor, Michigan 48104
(Received 27 June 1973)

We present new data on the η' meson based on 1414 η' events obtained from a 1 100 000-picture exposure of the BNL 31-inch hydrogen bubble chamber to a 2.18-GeV/c K^- beam. We have measured the η' mass, width, and branching ratios. We find that the very-forward-produced η' mesons have anisotropic angular distributions with respect to the incident K^- beam, suggesting that possibly $J^{PC}=2^{-+}$; however, the standard Dalitz-plot analyses favor $J^{PC}=0^{-+}$ over 2^{-+}.

I. INTRODUCTION

We report a study of the η' meson decaying into the modes (1) $\pi^+\pi^-\eta_N$, (2) $\pi^+\pi^-\eta_C$, (3) $\pi^+\pi^-\gamma$, and (4) all neutrals. The subscripts N and C refer to the η-decay modes $\eta \to$ neutrals and $\eta \to \pi^+\pi^-\pi^0$, $\pi^+\pi^-\gamma$, respectively. This study is based on 1.1×10^6 pictures (approximately 40 events/μb) of the hydrogen-filled 31-inch BNL bubble chamber, with an admixture of 4-mole-percent neon. The chamber was exposed to a 2.18-GeV/c K^- beam at the Brookhaven AGS in three runs.

The η' was discovered in 1964[1] and has been the subject of a number of subsequent investigations.[2-7]

The η' is known to be produced preferentially at low t (momentum transfer squared) in the reaction $K^-p \to \Lambda\eta'$,[1] and the scanning instructions for this experiment take advantage of this fact. Only events with a low-energy Λ decaying visibly into $p\pi^-$ are selected and this limits the scanning to unbiased events in which the momentum transfer squared from the target proton to the Λ is less than ≈ 0.8 GeV^2 in magnitude. In the analysis below we have imposed the more restrictive cut $|t| < 0.7$ GeV^2; this reduces the η' signal very little. Some preliminary results based on about 85% of the data have been reported previously.[8]

II. SELECTION OF EVENTS

A. The Final States $\Lambda\pi^+\pi^-\eta_N$, $\Lambda\pi^+\pi^-$ MM (for the Decays $\eta' \to \pi^+\pi^-\eta_N$, $\pi^0\pi^0\eta_C$)

The final-state assignment $\Lambda\pi^+\pi^-\eta_N$ means a successful fit with the mass of the missing neutral system equal to that of the η; MM means a missing neutral system with missing mass greater than two π^0 masses. Figure 1(a) is a plot of the mass recoiling against the Λ vs the unfitted missing-mass squared; it contains 4025 events. Only one of the interpretations $\Lambda\pi^+\pi^-\eta_N$, $\Lambda\pi^+\pi^-$MM is used per event, and if both are possible, only $\Lambda\pi^+\pi^-\eta_N$ is used. In the case of $\Lambda\pi^+\pi^-\eta_N$, the abscissa shows the *fitted* $\pi^+\pi^-\eta_N$ mass; the ordinate always is the unfitted MM^2. The cluster near the middle of this plot contains about 650 events and is evidence of the final state $\Lambda\eta'$, $\eta' \to \pi^+\pi^-\eta_N$; almost all the events in the cluster have a fit to $\Lambda\pi^+\pi^-\eta_N$. Fig-

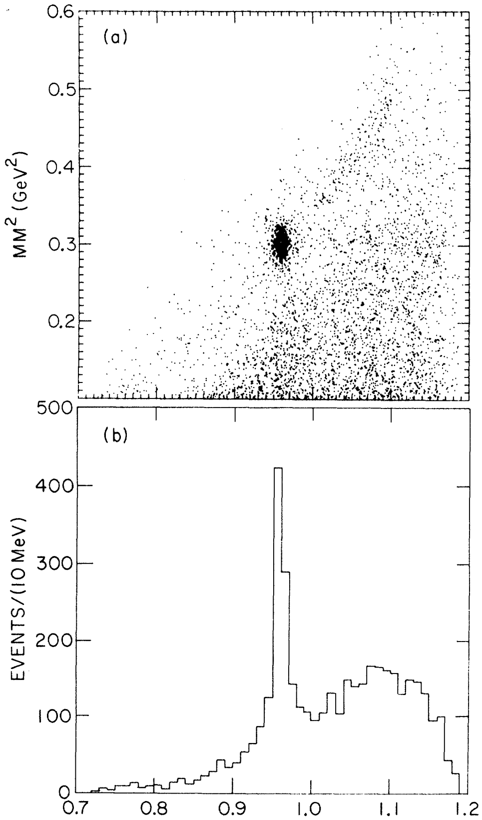

FIG. 1. (a) Scatter plot of unfitted MM^2 vs recoil mass for $K^-p \to \Lambda\pi^+\pi^-\eta$ (or MM). (b) Mass projection of (a) showing $\eta' \to \pi^+\pi^-\eta_N$.

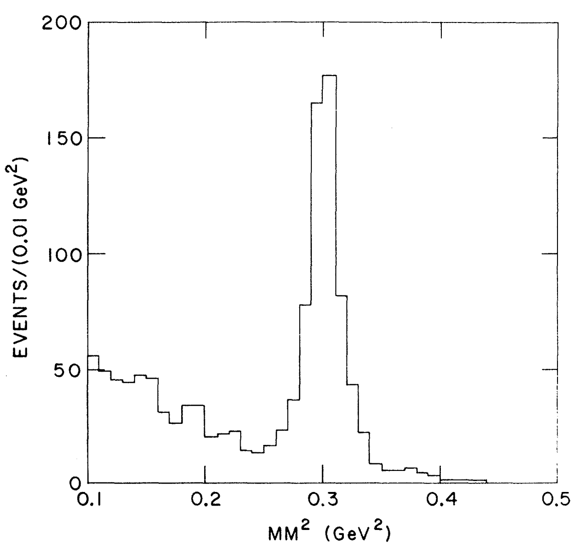

FIG. 2. MM^2 projection for events of Fig. 1(a) in η' band (930–990 MeV).

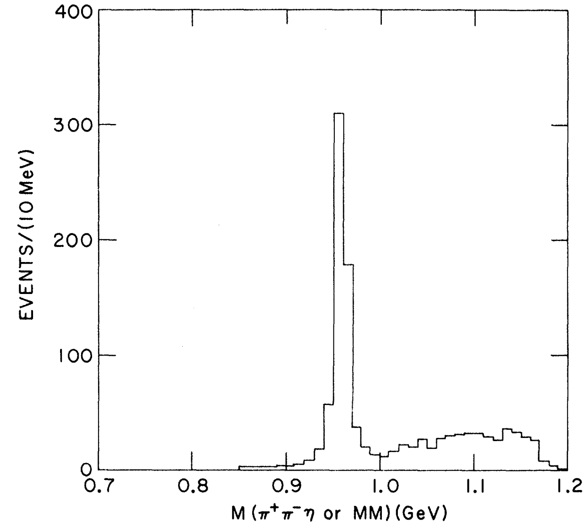

FIG. 3. Mass projection for events of Fig. 1(a) in η band [$MM^2 = (0.301 \pm 0.04)$ GeV^2].

ure 1(b) is the distribution of the mass of the system recoiling against the Λ, showing a clear η' signal. Figure 2 shows the distribution of missing mass squared for events in the η' band [930 MeV $< M(\pi^+\pi^-\eta_N$ or MM$) <$ 990 MeV] of Fig. 1(b); a peak at $MM^2 = m^2(\eta) \simeq 0.3$ GeV^2 is very clear. In Fig. 3 is shown the distribution of recoil mass for events in the η band ($|MM^2 - 0.301| < 0.04$ GeV^2) of Fig. 1(b).

For the analysis of the final state $\Lambda\pi^+\pi^-\eta_N$ we choose those events in the plot of Fig. 1(b) which satisfy $|MM^2 - 0.301| \leq 0.04$ GeV^2, and for the study of the decay mode $\eta' \to \pi^+\pi^-\eta_N$ we will impose the further restriction 930 MeV $< M(\pi^+\pi^-\eta_N$ or MM) $<$990 MeV. We estimate that no events are lost from the decay mode $\eta' \to \pi^+\pi^-\eta_N$ due to the MM^2 cuts.

A complication is the fact that a substantial fraction of the events in the decay mode

$$\eta' \to \pi^0\pi^0\eta_C, \quad \eta_C \to \pi^+\pi^-\pi^0 \text{ or } \gamma \tag{2.1}$$

are included by the above missing-mass-squared cut designed to isolate the decay mode $\eta' \to \pi^+\pi^-\eta_N$. This is because the two π^0's from $\eta' \to \pi^0\pi^0\eta_C$ and the neutral particle from the subsequent decay of the η_C have a mass spectrum which overlaps the region of the η mass. To see what fraction of the $\eta' \to \pi^0\pi^0\eta_C$ events are included by the above missing-mass-squared cut, we examine events from the decay mode $\eta' \to \pi^+\pi^-\eta_C$, which should behave the same as $\eta' \to \pi^0\pi^0\eta_C$ events. We denote the final-state particles by subscripts 1 and 2, and write

$$\eta' \to \pi_1^+\pi_1^-\eta_C, \quad \eta_C \to \pi_2^+\pi_2^-\pi^0 \text{ or } \gamma\,. \tag{2.2}$$

The distribution of $M^2(\pi_1^+, \pi_1^-, \pi^0$, or $\gamma)$ should be the

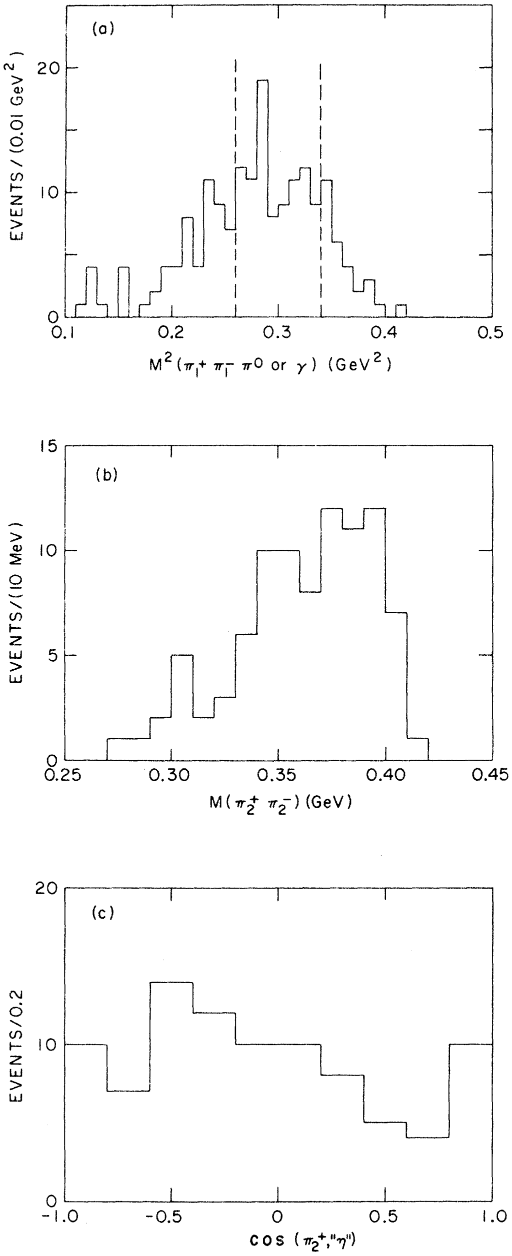

FIG. 4. The $\eta' \rightarrow \pi_1^+\pi_1^-\eta_C$ events misidentified so as to "fake" $\eta' \rightarrow \pi^0\pi^0\eta_C$ (see text). (a) $M^2(\pi_1^+\pi_1^-\pi^0$ or $\gamma)$ distribution where $M^2(\pi_2^+\pi_2^-\pi^0$ or $\gamma)$ is the "true" η(548 MeV). (b) The $\pi_2^+\pi_2^-$ mass distribution corresponding to the cut indicated in (a). (c) Dalitz-plot decay cosine for the events of (b).

same as that of the three neutral particles in (2.1). This distribution is shown in Fig. 4(a); the dashed lines indicate the cut around the mass squared of the η used for Fig. 3. From Fig. 4(a) we find that $(51 \pm 4)\%$ of the events from (2.1) are included in the sample of events called $\eta' \rightarrow \pi^+\pi^-\eta_N$. From isospin considerations $[I(\eta')=0]$ and the known

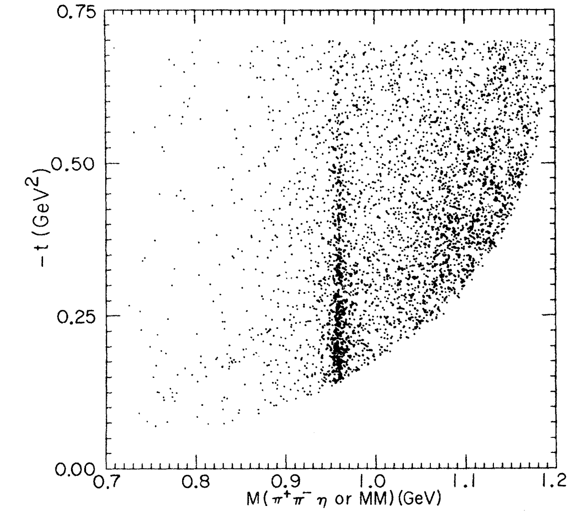

FIG. 5. Chew-Low scatter plot of $\Lambda\pi^+\pi^-(\eta$ or MM) events; note strong η' band.

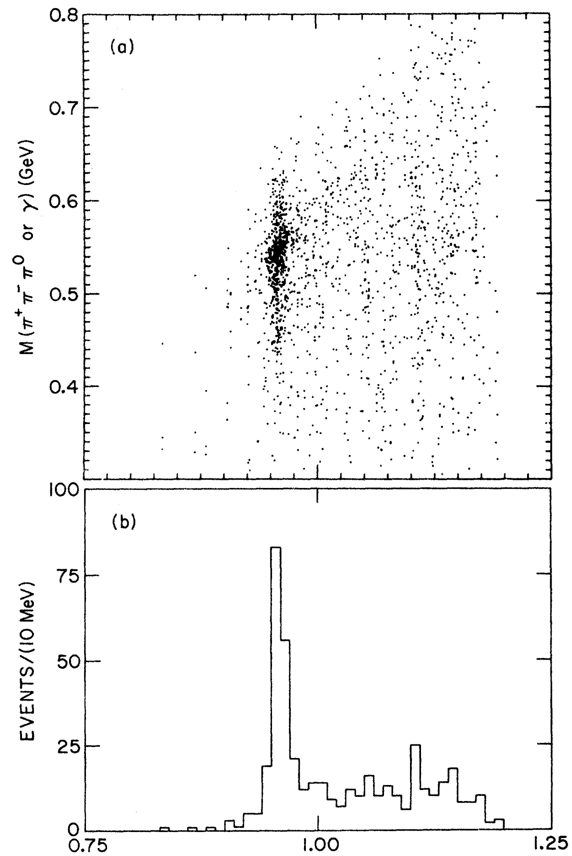

FIG. 6. (a) Scatter plot of $M(\pi^+\pi^-\pi^0)$ vs recoil mass for $K^-p \rightarrow \Lambda\pi^+\pi^+\pi^-\pi^-\pi^0$ (or γ) events (4 combinations per event). (b) Recoil mass projection of (a) showing η' peak (once per event).

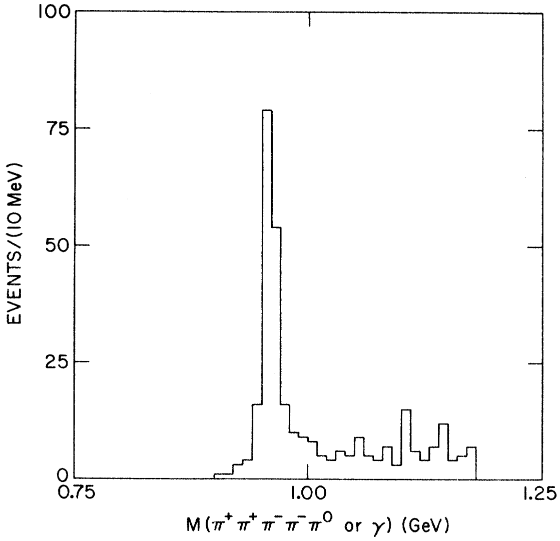

FIG. 7. Recoil mass projection of events of Fig. 6(a) in η band [$M^2(\pi^+\pi^-\pi^0$ or $\gamma) = (549 \pm 25)$ MeV] (once per event).

$\eta(549)$ branching ratios[9] we conclude that $(9 \pm 1)\%$ of the events called $\eta' \to \pi^+\pi^-\eta_N$ are actually $\eta' \to \pi^0\pi^0\eta_C$ events. This will be taken into account below when the η' branching ratios are calculated. The misidentified $M(\pi\pi)$ and $\cos\theta_{\pi\eta}$ distributions from $\pi^0\pi^0\eta_C$ events, Figs. 4(b) and 4(c), will be used below when we consider the effect of $\eta' \to \pi^0\pi^0\eta_C$ events on the quantum-number determination of the $\eta' \to \pi^+\pi^-\eta_N$ events.

Figure 5 is a Chew-Low plot for events of Fig. 1. The peripheral nature of the η' production is clear and it is apparent that the cut $|t| < 0.7$ GeV^2 excludes very few η' events.

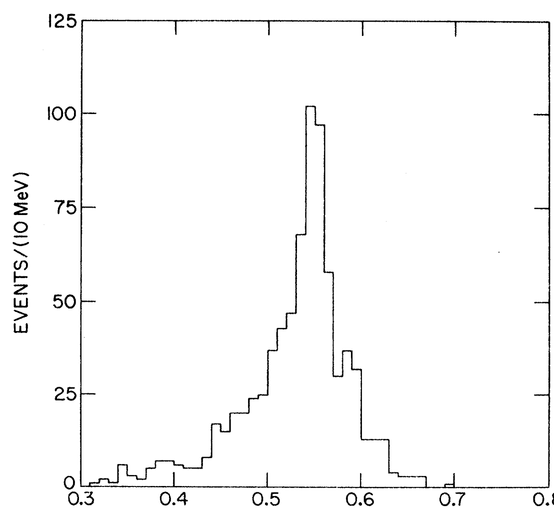

FIG. 8. $M(\pi^+\pi^-\pi^0$ or $\gamma)$ mass projection for events of Fig. 6(a) in η' band (930–990 MeV).

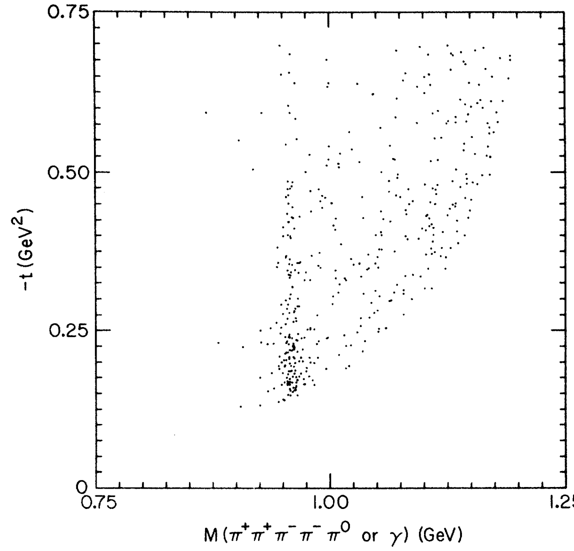

FIG. 9. Chew-Low scatter plot of $\Lambda\pi^+\pi^+\pi^-\pi^-\pi^0$ (or γ) events; note strong η' band.

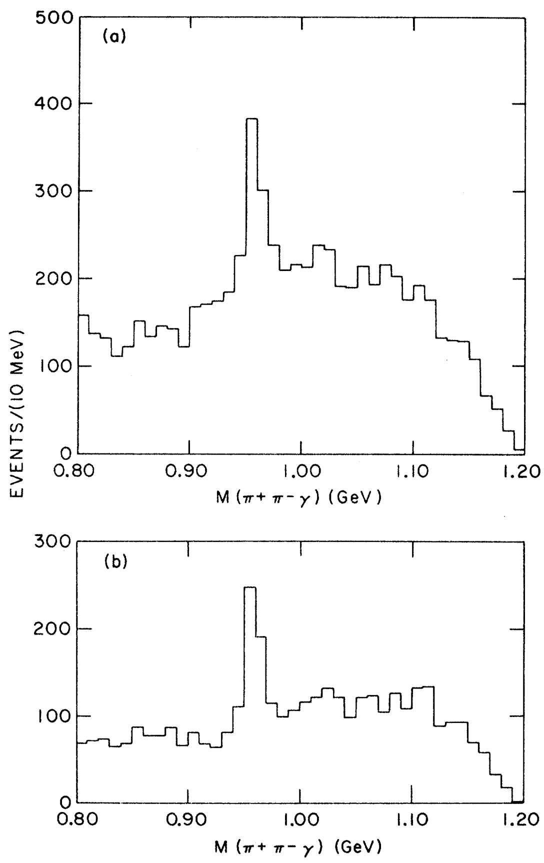

FIG. 10. (a) Recoil mass distribution $M(\pi^+\pi^-\gamma)$ for an "enriched" sample (see text) of $K^-p \to \Lambda\pi^+\pi^-\gamma$ events. (b) Same for events with $620 < M(\pi^+\pi^-) < 880$ MeV (ρ band).

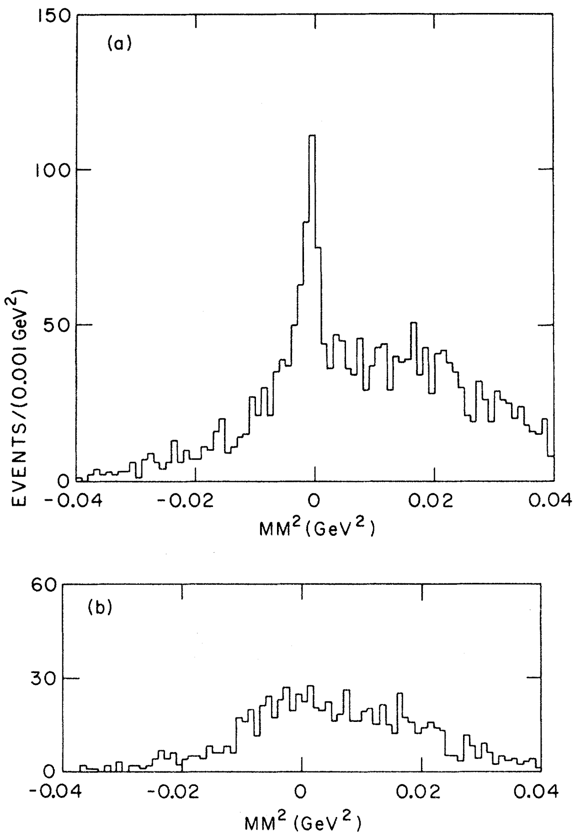

FIG. 11. (a) Missing mass squared, MM^2, distribution for $\Lambda\pi^+\pi^-\gamma$ having $930 < M(\pi^+\pi^-\gamma) < 990$ MeV. (b) Same for events with $620 < M(\pi^+\pi^-) < 880$ MeV (ρ band).

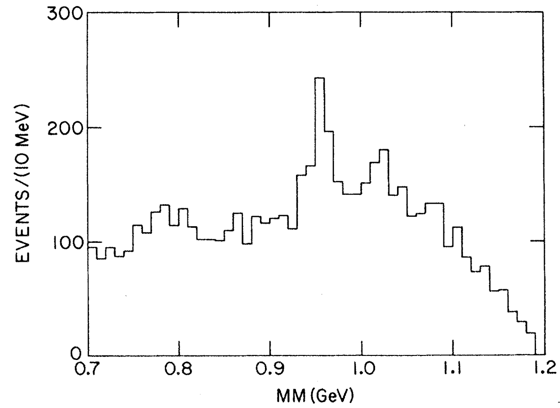

FIG. 13. Missing mass, MM, histogram for Λ + neutrals, showing $\eta' \to$ all neutrals.

B. The Final States $\Lambda\pi^+\pi^+\pi^-\pi^-\pi^0$, $\Lambda\pi^+\pi^+\pi^-\pi^-\gamma$ (for the Decay $\eta' \to \pi^+\pi^-\eta_C$)

All events fitting these final states were analyzed for η' production except for those events which had a confidence level greater than 0.1 for a fit to $\Lambda\pi^+\pi^+\pi^-\pi^-$ or to $\Sigma^0\pi^+\pi^+\pi^-\pi^-$. An examination of the excluded events showed that only (13 ± 5) η' events were lost by this cut. When both $\Lambda\pi^+\pi^+\pi^-\pi^-\pi^0$ and $\Lambda\pi^+\pi^+\pi^-\pi^-\gamma$ fit, the assignment to one of these final states was made on the basis of a missing-mass-squared cut. The missing neutral was called a γ for $\mathrm{MM}^2 < 0.005$ GeV^2, or a π^0 if $\mathrm{MM}^2 > 0.005$ GeV^2. This cut was found to give an acceptable ratio of $\eta \to \pi^+\pi^-\gamma$ to $\eta \to \pi^+\pi^-\pi^0$ decays of 0.3 ± 0.1 observed vs 0.2 expected[9] for events chosen as $\Lambda\eta'$, $\eta' \to \pi^+\pi^-\eta_C$. The distribution of $M(\pi^+\pi^+\pi^-\pi^-\pi^0$ or $\gamma)$ in Fig. 6(b) shows a strong η'

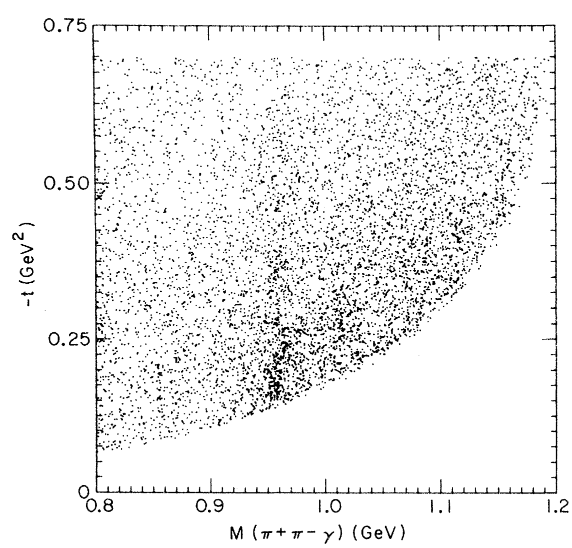

FIG. 12. Chew-Low scatter plot of $\Lambda\pi^+\pi^-\gamma$ events; note η' band.

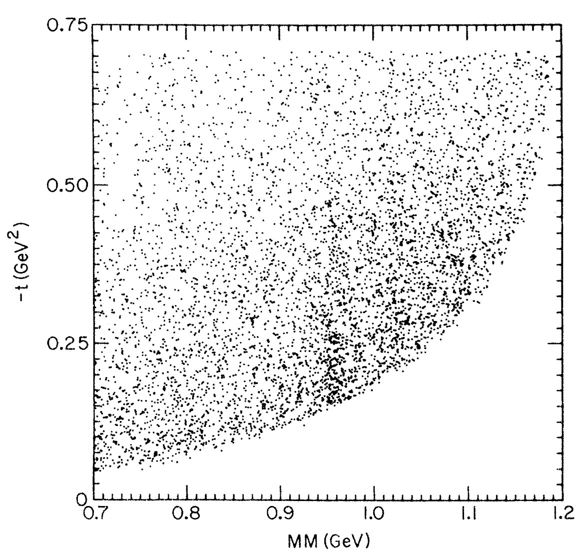

FIG. 14. Chew-Low scatter plot of Λ + neutrals events; η' band evident.

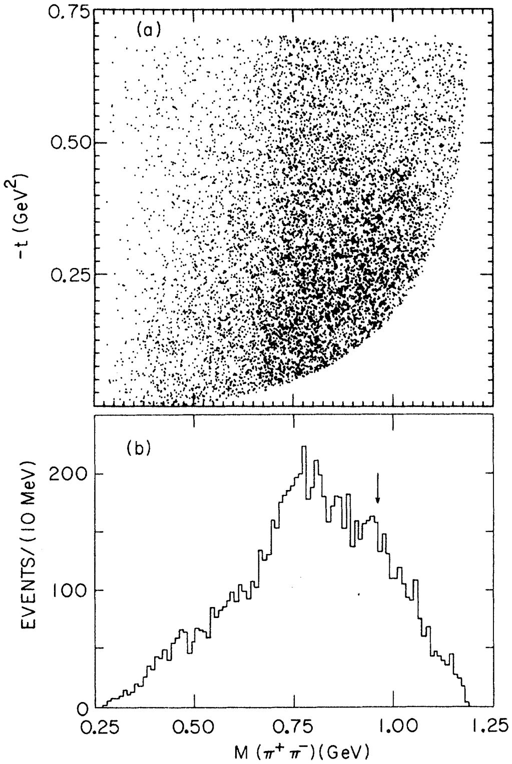

FIG. 15. (a) Chew-Low scatter plot of $\Lambda\pi^+\pi^-$ events. (b) $M(\pi^+\pi^-)$ projections of (a); the arrow indicates 960 MeV; no η' observed.

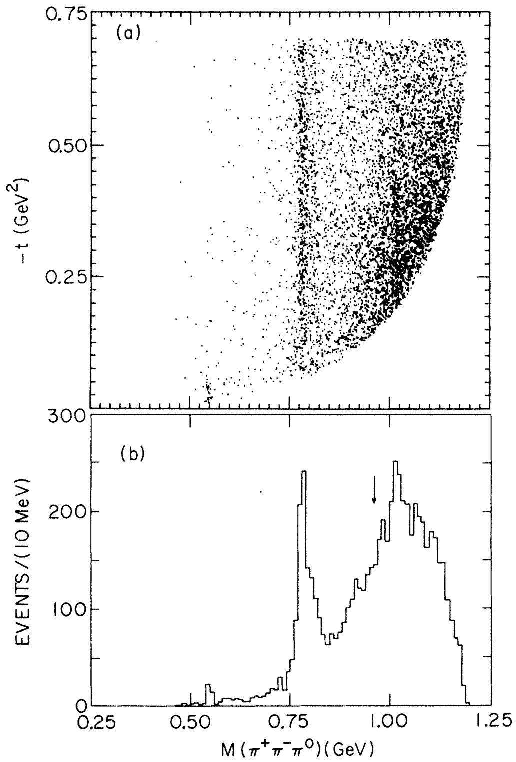

FIG. 16. (a) Chew-Low scatter plot of $\Lambda\pi^+\pi^-\pi^0$ events with $MM^2 > 0.018$ GeV^2. (b) $M(\pi^+\pi^-\pi^0)$ projection of (a); arrow indicates 960 MeV; no η' observed.

signal. When an η_c cut is imposed [at least one $M(\pi^+\pi^-\pi^0$ or $\gamma)$ combination within 25 MeV of 549 MeV], the background under the η' signal is reduced even more; this is shown in Fig. 7. The η signal in the η' mass band [930 MeV $< M(\pi^+\pi^+\pi^-\pi^-\pi^0$ or $\gamma)$ $<$990 MeV] is also very prominent, as displayed in Fig. 8. Figure 9 shows the Chew-Low plot for all the events of Fig. 6; again the peripheral nature of the η' signal is evident.

C. The Final State $\Lambda\pi^+\pi^-\gamma$ (for the Decay $\eta' \to \pi^+\pi^-\gamma$)

The final state $\Lambda\pi^+\pi^-\gamma$ is difficult to separate from the channels $\Lambda\pi^+\pi^-$, $\Sigma^0\pi^+\pi^-$, and $\Lambda\pi^+\pi^-\pi^0$ because of the proximity of the missing mass for these four reactions. Since it will be shown below that the η' does not decay into $\pi^+\pi^-$ or $\pi^+\pi^-\pi^0$, we discuss now only those events fitting the final state $\Lambda\pi^+\pi^-\gamma$. All events fitting $\Lambda\pi^+\pi^-\gamma$ were analyzed, except those for which (1) $MM^2 > 0.018$ GeV^2 and (2) $\Lambda\pi^+\pi^-$ or $\Sigma^0\pi^+\pi^-$ fits with confidence level $>$0.1 and $M(\Lambda\gamma) \approx M(\Sigma^0) = (1.92 \pm 0.025)$ GeV. The first cut excludes many $\Lambda\pi^+\pi^-\pi^0$ events, losing essentially no $\Lambda\pi^+\pi^-\gamma$ events. The second cut excludes most $\Lambda\pi^+\pi^-$ and $\Sigma^0\pi^+\pi^-$ events, but also excludes about 25% of the $\eta' \to \pi^+\pi^-\gamma$ signal. This enriched sample of $\Lambda\pi^+\pi^-\gamma$ events is used for analysis of the η' properties. The second cut is modified later in making branching-ratio estimates.

Figure 10(a) shows the mass spectrum of the $\pi^+\pi^-\gamma$ for the events left after applying the above cuts; the spectrum of Fig. 10(b) is that for $M(\pi^+\pi^-)$ in the ρ-meson band [$M(\pi^+\pi^-) = (750 \pm 130)$ MeV]. Most of the events shown are really $\Lambda\pi^+\pi^-\pi^0$, but a clear η' signal at about 960 MeV is present. That it is associated with $\Lambda\pi^+\pi^-\gamma$ and not with $\Lambda\pi^+\pi^-\pi^0$ is shown by the MM^2 plot of Fig. 11(a) for events in the η' band [930 MeV $< M(\pi^+\pi^-\gamma) <$990 MeV]. The narrow peak at $MM^2 = 0$ is due to $\Lambda(\Sigma^0)\pi^+\pi^-$ remaining in the accepted $\Lambda\pi^+\pi^-\gamma$ sample. The events of Fig. 11(b) are those $\Lambda\pi^+\pi^-\gamma$ events having $M(\pi^+\pi^-)$ in the ρ-meson region [0.62 GeV $< M(\pi^+\pi^-) <$0.88 GeV], and give a peak at $MM^2 = 0$. $\Lambda\pi^+\pi^-\pi^0$ events in general give a MM^2 distribution peaked at 0.018 GeV^2. The Chew-Low plot of Fig. 12 again shows that the η' signal occurs for low values of $|t|$.

D. The Final State (Λ+Neutrals) (for the Decay $\eta' \to$ Neutrals)

Figure 13 is a plot of the mass of the neutrals recoiling against the Λ. A clear η' signal is seen near the mass value 960 MeV, and a smaller ϕ signal is evident near 1020 MeV. The Chew-Low plot of Fig. 14 demonstrates the peripheral nature of the η' production.

E. The Final State $\Lambda\pi^+\pi^-$ (No Evidence for $\eta'\to\pi^+\pi^-$)

Figure 15 contains data from events fitting $\Lambda\pi^+\pi^-$ with a confidence level greater than 10^{-3}. Figure 15(a) is a Chew-Low plot, and Fig. 15(b) is the distribution of $M(\pi^+\pi^-)$. The arrow denotes the expected position of an η' signal; none is present.

F. The Final State $\Lambda\pi^+\pi^-\pi^0$ (No Evidence for $\eta'\to\pi^+\pi^-\pi^0$)

Figure 16 is for events fitting $\Lambda\pi^+\pi^-\pi^0$. Only events with $MM^2 > 0.018$ GeV^2 are displayed here to avoid confusion with $\Lambda\pi^+\pi^-\gamma$. Neither the Chew-Low plot of Fig. 16(a) nor the mass plot of Fig. 16(b) show evidence for $\eta'\to\pi^+\pi^-\pi^0$. The arrow in Fig. 16(b) marks the expected position of an η' signal.

G. The Final State $\Lambda\pi^+\pi^+\pi^-\pi^-$ (No Evidence for $\eta'\to\pi^+\pi^+\pi^-\pi^-$)

Events fitting $\Lambda\pi^+\pi^+\pi^-\pi^-$ were selected for Fig. 17. Again neither the Chew-Low plot [Fig. 17(a)] nor the mass plot [Fig. 17(b)] contains evidence

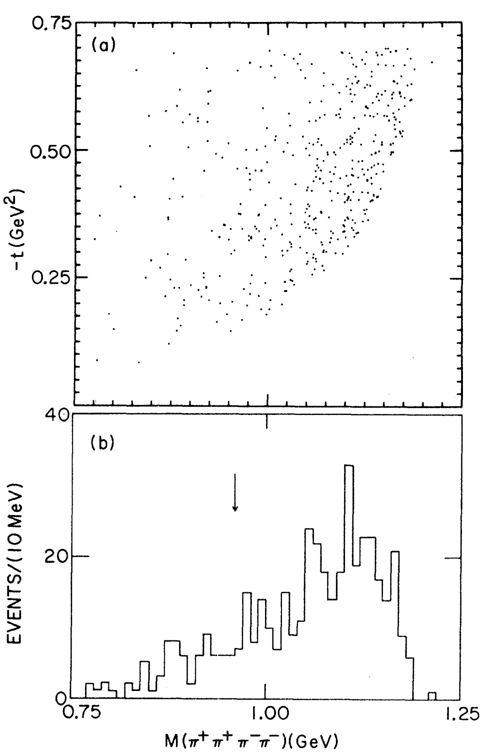

FIG. 17. (a) Chew-Low scatter plot of $\Lambda\pi^+\pi^+\pi^-\pi^-$ events. (b) $M(\pi^+\pi^+\pi^-\pi^-)$ projection of (a); arrow indicates 960 MeV; no η' observed.

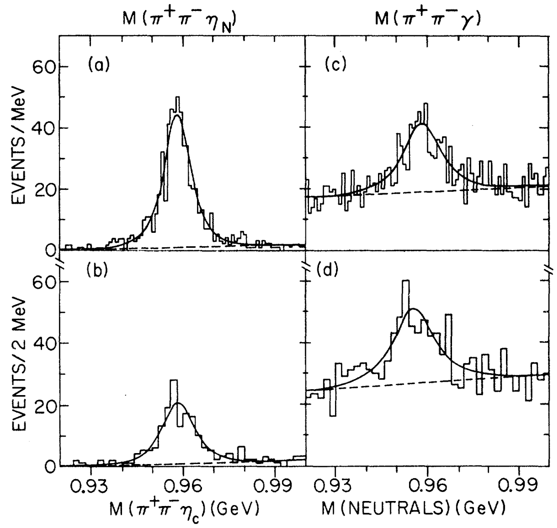

FIG. 18. Recoil mass distributions for four final states from 900–1020 MeV with best fit curves for mass and width determination (see text) (a) for $\pi^+\pi^-\eta_N$; (b) for $\pi^+\pi^-\eta_C$; (c) for $\pi^+\pi^-\gamma$; and (d) for all neutrals.

for $\eta'\to\pi^+\pi^+\pi^-\pi^-$; the expected η' signal position is marked by an arrow.

III. η' MASS, WIDTH, AND BRANCHING RATIOS

The mass spectra of Figs. 3, 7, 10, and 13 were fitted with Breit-Wigner resonance curves folded with the expected resolution broadening to estimate the mass, width, and numbers of η' events in the various final states. The procedure used was essentially the same as that described in Borenstein *et al.*[10] For each of the final states $\Lambda\pi^+\pi^-\eta_N$, $\Lambda\pi^+\pi^-\eta_C$, $\Lambda\pi^+\pi^-\gamma$, Λ + neutrals, those events were considered which lay in a meson mass band from 920 to 1000 MeV centered around the η' mass. The distribution of errors in the meson mass was used to generate a resolution function; the resolution function was subsequently fitted to the functional form

$$f(M)=\left[\sum_{n=0}^{3} a_n (M)^{2n}\right]^{-1} . \tag{3.1}$$

The resolution function was broadened by an overall scale factor if it was found that the errors had been incorrectly estimated. To determine whether the errors had been correctly estimated, a plot of the confidence-level distribution was made for each of the event samples, for various values of a factor f^2 multiplying each kinematic χ^2 value for the fit. A value of f^2 was found which yielded the most nearly flat confidence-level distribution, and the corresponding value of f^{-1} was used to scale the resolution function described above. All the values of f^{-1} were near 1.1. The error in f was folded in-

TABLE I. η' mass (M) and width (Γ).

Channel	f	$\Gamma_R = \Gamma^*_{calc} f^{-1}$ (MeV) (FWHM)	$\Gamma_{observed}$ (MeV) (FWHM)	Background	Best fit M (MeV)	Best fit Γ (MeV)	Corrected[b] M (MeV)	Γ (MeV) upper limit (90% C.L.)
$\eta' \to \pi^+\pi^-\eta_N$	0.86 ± 0.01	9.9	9	Quadratic	958.3 ± 0.2	1.7	958.3 ± 0.6	≤ 4.4[c]
$\eta' \to \pi^+\pi^-\eta_C$	0.89 ± 0.02	11.7	12	Quadratic	958.4 ± 0.7	1.4	958.4 ± 0.8	≤ 7
$\eta' \to \pi^+\pi^-\gamma$	0.86 ± 0.01[a]	9.9[a]	~16	Linear	958.0 ± 0.7	2	958.0 ± 0.8	≤ 13
$\eta' \to$ neutrals	0.94 ± 0.02	17	~20	Linear	955.3 ± 0.9	2	955.3 ± 1.2[b]	≤ 20[d]
					Best values:		(958.2 ± 0.5) MeV, (wtd. avg.)	≤ 4.4 MeV[c]

[a] Taken to be same as $\eta' \to \pi^+\pi^-\eta_N$.

[b] All are corrected for a systematic mass shift of (0 ± 0.5) MeV (see text); in addition $\eta' \to$ neutrals is corrected by (0 ± 0.5) MeV for lack of constrained production-vertex fit.

[c] ≤ 4.7 MeV (95% C.L.).

[d] The observed width.

to the uncertainty in the η' width determination.

The scaled resolution function obtained in this manner was folded with a Breit-Wigner line shape for the η' decay and superimposed on a presumed linear (or quadratic) background to fit the mass spectrum being considered. Figure 18 shows the best fits superimposed on the mass plots for each of the four final states. In each case the width of the η' was consistent with zero. The mass and width results are summarized in Table I. All the mass values are corrected for a systematic mass shift of (0 ± 0.5) MeV as determined from the comparison of the mass values of the η, ω, and ϕ observed in our data with the standard values.[9] In addition the all-neutral decays are corrected by (0 ± 0.5) MeV for lack of a constrained production-vertex fit again as determined by the observed masses of all neutral decays of the η, ω, and ϕ as compared to their charged decays. The width values are 90%-confidence-level upper limits and include both the statistical uncertainty and the uncertainty in the resolution function. The confidence-level distribution versus assumed width is shown in Fig. 19 for the $\eta' \to \pi^+\pi^-\eta_N$ decay mode.

The numbers of events in each of the η' decay modes are given in Table II. The number of $\eta' \to \pi^+\pi^-\gamma$ events was not determined from the data of Fig. 10 but from a similar distribution (not shown) containing all $\Lambda\pi^+\pi^-\gamma$ events except those also fitting $\Lambda\pi^+\pi^-$. The η' width was held constant at 2 MeV in order to keep the estimates of the background under reasonable control. In each case the numbers of events are corrected for losses due to the cuts described above and for the relative scanning and computer processing efficiencies of the various event topologies.

The η' branching ratios have been determined using the numbers of events in the final states $\eta' \to \pi^+\pi^-\eta_N$ and $\eta' \to \pi^+\pi^-\gamma$ only. This was done because these two modes are subject to the same scanning and computer-processing biases. Using as input the branching ratio of 1.7% for the decay

TABLE II. Numbers of η' events (η' width fixed at 2 MeV)

Channel	Number of events above background	Correction factors: Scanning[d]	Correction factors: Processing[e]	Corrected no. of events	Number expected from $\pi^+\pi^-\eta_N$
$\eta' \to \pi^+\pi^-\eta_N$	514 ± 25[a]	1	1		
$\eta' \to \pi^+\pi^-\eta_C$	163 ± 17[b]	1	1.06 ± 0.04	173 ± 19	198 ± 13
$\eta' \to \pi^+\pi^-\gamma$	473 ± 66[c]	1	1		
$\eta' \to$ neutrals	264 ± 50	1.02 ± 0.11	0.98 ± 0.01	264 ± 60	282 ± 15[f]
	1414 ± 86				

[a] 0.91×564 ($\pi^+\pi^-\eta_N + \pi^0\pi^0\eta_C$) events.

[b] (150 ± 16) events + (13 ± 5) events lost by cuts (see text).

[c] From histogram (not shown) similar to Fig. 10, but *not* excluding $\Sigma^0\pi^+\pi^-$ final state.

[d] Determined from $\eta, \omega, \phi \to$ neutrals vs $\eta, \omega, \phi \to$ charged decays.

[e] Determined from number of events passing geometry vs number found by scanners.

[f] Includes (25 ± 5) $\gamma\gamma$ events corresponding to a $\gamma\gamma$ branching ratio of (1.7 ± 0.3)% (see Ref. 6).

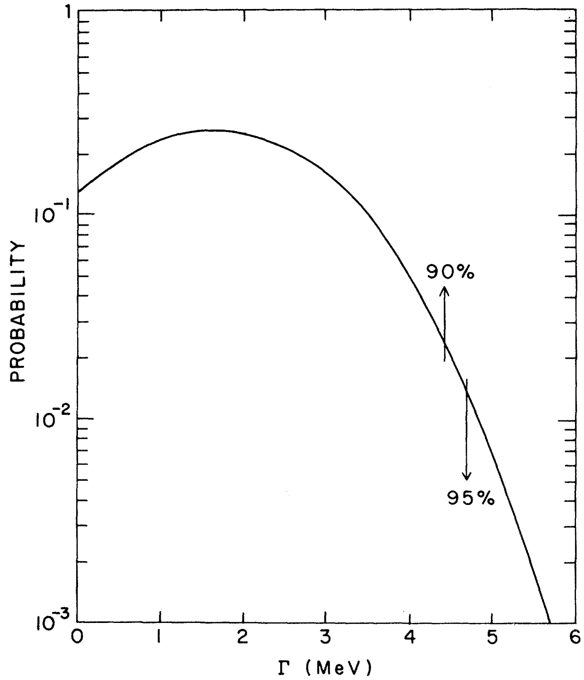

FIG. 19. Confidence level (logarithm of probability) vs assumed true η' width Γ for $\Lambda\pi^+\pi^-\eta_N$ events. The arrows mark the 90-to-95-percent-confidence-level upper limits, respectively.

$\eta' \to \gamma\gamma$,[6,9] we obtain the branching ratios shown in Table III. In addition we give the 95%-confidence-level upper limits for the decays $\eta' \to \pi^+\pi^-$, $\pi^+\pi^-\pi^0$, and $\pi^+\pi^-\pi^-\pi^-$ derived from the data in Figs. 15, 16, and 17, respectively. That $\eta' \to \pi^+\pi^-\gamma$ is actually $\eta' \to \rho^0\gamma$ is seen from the events in Fig. 10(b) and in the analyses of Sec. IV. We note at this point that the numbers of events in the various decay modes listed in Table II are consistent with one another, within errors.

TABLE III. η' branching ratios.

$\Gamma(\pi^+\pi^-\gamma)/\Gamma(\pi^+\pi^-\eta_N)$	0.92 ± 0.14
$\Gamma(\rho\gamma)/\Gamma(\pi^+\pi^-\gamma)$	1.15 ± 0.10 [a]
$\Gamma(\pi\pi\eta)/\Gamma(\text{all})$	0.681 ± 0.032
$\Gamma(\pi^+\pi^-\gamma)/\Gamma(\text{all})$	0.302 ± 0.032
$\Gamma(\gamma\gamma)/\Gamma(\text{all})$	0.017 ± 0.0033 (input) [b]
$\Gamma(\pi^+\pi^-)/\Gamma(\text{all})$	<0.08 (95% C.L.) [c]
$\Gamma(\pi^+\pi^-\pi^0)/\Gamma(\text{all})$	<0.09 (95% C.L.) [d]
$\Gamma(\pi^+\pi^+\pi^-\pi^-)/\Gamma(\text{all})$	<0.01 (95% C.L.) [c]

[a] Number of $\pi^+\pi^-\gamma$ with $0.62 < M(\pi^+\pi^-) < 0.88$ GeV compared to 0.82 times the total number of $\pi^+\pi^-\gamma$ events (the expectation from the $J^P = 0^-$ matrix element). This corresponds to $\Gamma(\rho\gamma)/\Gamma(\pi^+\pi^-\gamma) > 0.95$ (95% confidence limit).

[b] See Ref. 6.

[c] Upper limits of number of excess events in mass region 940–980 MeV compared to those in 920–940 and 980–1000 MeV (linear extrapolation) from Fig. 15 ($\pi^+\pi^-$) and Fig. 17 ($\pi^+\pi^+\pi^-\pi^-$).

[d] Two times upper limit of excess events as in Ref. c for data of Fig. 16 ($\pi^+\pi^-\pi^0$) to compensate for cut on $MM^2 > 0.018$ GeV^2.

Our final value for the η' mass, (958.2 ± 0.5) MeV, agrees with previous determinations,[9] as do the $\pi\pi\eta$ and $\pi^+\pi^-\gamma$ branching ratios.[9] Our width upper limit (90% confidence level) of 4.4 MeV is to be compared with the upper limits of 4 MeV, based on events from an early experiment,[2] and of 2.8 MeV (revised) from a recent counter experiment.[11]

IV. η' QUANTUM NUMBERS

A. Dalitz-Plot Analyses

To determine the η' quantum numbers we have first fitted the Dalitz-plot distributions for the de-

TABLE IV. Matrix elements M for $\eta' \to \pi^+\pi^-\eta$. l_η is the orbital angular momentum of the η in the η' rest frame, and $l_{\pi\pi}$ is that of the two pions in the $\pi\pi$ rest frame. $\vec{k}$ is the η momentum in the η' rest frame, and $\vec{q} = \frac{1}{2}(\vec{p}_{\pi^+} - \vec{p}_{\pi^-})$ in the $\pi\pi$ rest frame. θ is the angle between the directions of the π^+ and the η in the $\pi\pi$ rest frame. $|M|^2$ is summed over spins.

Quantum numbers	$l_\eta, l_{\pi\pi}$	$\lvert M\rvert^2$
$C=+$, $J^P=0^-$	0, 0	1
$J^P=1^+$	1, 0	k^2
$J^P=1^-$	2, 2	$q^4k^4\cos^2\theta\sin^2\theta$
$J^P=2^+$	1, 2	$q^4k^2\sin^2\theta$
$J^P=2^-$	0, 2	q^4
$J^P=2^-$	2, 0	k^4
$J^P=2^-$ mixture	$M(l_\eta=0)+aM(l_\eta=2)$	$q^4+\mathrm{Re}(a)q^2k^2(3\cos^2\theta-1)+\lvert a\rvert^2k^4$
$J^P=2^-$	2, 2	$q^4k^4\cos^2\theta(3+\cos^2\theta)$
$C=-$, $J^P=0^-$	1, 1	$q^2k^2\cos^2\theta$
$J^P=1^+$	0, 1	q^2
$J^P=1^-$	1, 1	$q^2k^2\sin^2\theta$
$J^P=2^+$	2, 1	$q^2k^4\sin^2\theta$
$J^P=2^-$	1, 1	$q^2k^2(3+\cos^2\theta)$

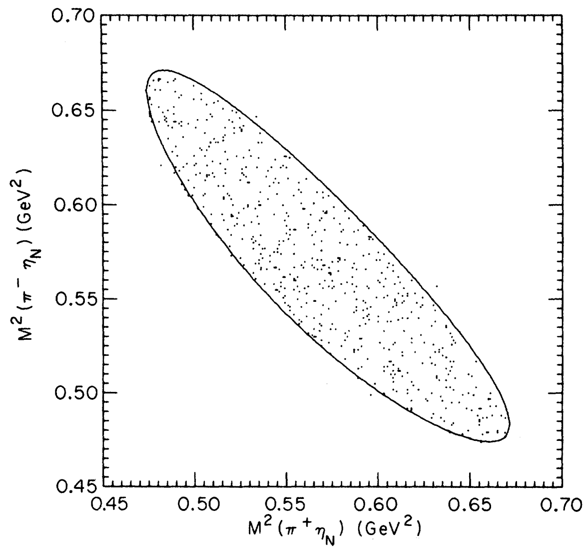

FIG. 20. Dalitz plot of $M^2(\pi^+\eta_N)$ vs $M^2(\pi^-\eta_N)$ for $\Lambda\pi^+\pi^-\eta_N$ events in the η' region.

cays $\eta' \to \pi^+\pi^-\eta_N$, $\pi^+\pi^-\eta_C$, $\pi^+\pi^-\gamma$ to the predictions of various quantum-number assignments for spin values of 0, 1, and 2.

The $\pi\pi\eta$ decays are characterized by the orbital angular-momentum values $l_{\pi\pi}$ (the relative orbital angular momentum of the two pions) and by l_η (the orbital angular momentum of the η with respect to the $\pi\pi$ system). Table IV shows the form of the squared matrix elements[3] for the C and J^P values that were fitted. For most of the $\pi\pi\eta$ decays only one choice of $l_{\pi\pi}$ and l_η is possible. For the $J^{PC} = 2^{-+}$ hypothesis, however, two choices are possible: $l_\eta = 0$, $l_{\pi\pi} = 2$; or $l_\eta = 2$, $l_{\pi\pi} = 0$. The $J^{PC} = 2^{-+}$ fits have been done for each choice separately, and for real and complex mixtures of the two possible matrix elements. For the $J^{PC} = 0^{-+}$ assignment we have also fitted the $\pi\pi\eta$ decays to the simplest matrix element multiplied by the term $(1+\alpha Y)$, where α is a parameter to be determined,

$$Y = (m_\eta + 2m_\pi)(T_\eta / m_\pi Q) - 1$$

is the y coordinate of the "triangular" Dalitz-Fabri plot,[3,12] and the other symbols have their usual meaning.

Figure 20 shows the $\eta' \to \pi^+\pi^-\eta_N$ Dalitz plot containing 621 events, about 10% of which are estimated to be background, and about 8% of which are estimated to come from the decay $\eta' \to \pi^0\pi^0\eta_C$. The events in the Dalitz plot are normalized to an η' mass of 958 MeV by calculating[3]

$$M^2(\pi^+,\eta)' = (M - m_{\pi^-})^2 + \frac{MQ_0}{M^f Q^f}\left[M^f(\pi^+,\eta)^2 - (M^f - m_{\pi^-})^2\right],$$

$$M^2(\pi^-,\eta)' = (M - m_{\pi^+})^2 + \frac{MQ_0}{M^f Q^f}\left[M^f(\pi^-,\eta) - (M^f - m_{\pi^+})^2\right],$$

TABLE V. $\eta' \to \pi^+\pi^-\eta_N$.

Matrix element	Conf. level [a]
$C=+$, $J^P=0^-$	0.46
$M(0^-)(1+\alpha Y) \to \alpha = -0.03 \pm 0.04$	
$J^P=1^+$	Excluded
$J^P=1^-$	Excluded
$J^P=2^+$	Excluded
$J^P=2^-$, $l_\eta=2$	Excluded
$J^P=2^-$, $l_\eta=0$	Excluded
$J^P=2^-$ mixture: $M(l_\eta=0)+aM(l_\eta=2)$	
$a=(-0.01\pm0.05)+(0.36\pm0.02)i$	0.22
$a(\text{real})=0.35\pm0.02$	3×10^{-5}
$C=-$, $J^P=0^-$	Excluded
$J^P=1^+$	Excluded
$J^P=1^-$	Excluded
$J^P=2^+$	Excluded
$J^P=2^-$	Excluded

[a] Excluded means conf. level less than 10^{-6}.

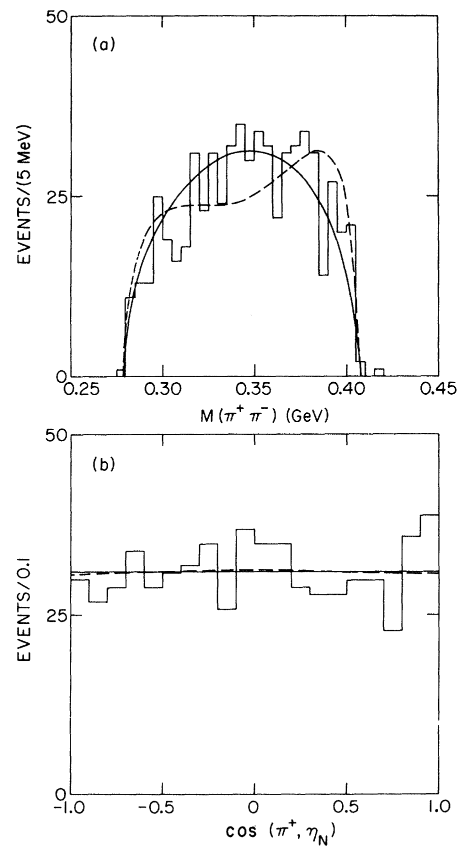

FIG. 21. (a) $M(\pi^+\pi^-)$ projection and (b) cosine (π^+, η_N) projection of Fig. 20. The solid curve represents the $J^P = 0^-$ fit, and the dashed curve the best $J^P = 2^-$ fit.

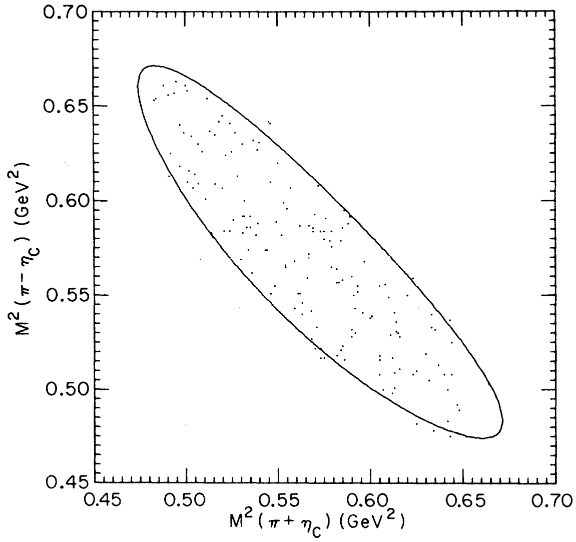

FIG. 22. Dalitz plot of $M^2(\pi^+\eta_C)$ vs $M^2(\pi^-\eta_C)$ for $\Lambda\pi^+\pi^-\eta_C$ events in the η' region.

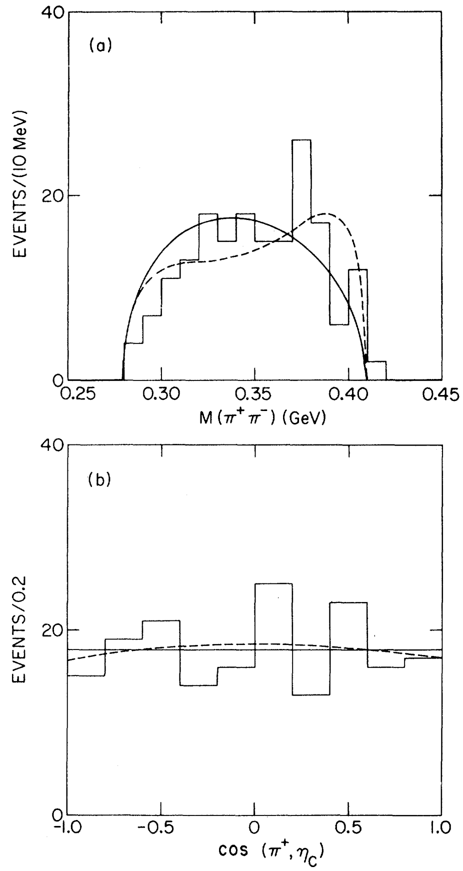

FIG. 23. (a) $M(\pi^+\pi^-)$ projection and (b) cosine (π^+, η_C) projection of Fig. 22. The solid curve represents the $J^P=0^-$ fit, and the dashed curve the best $J^P=2^-$ fit.

where M, Q_0 are the standard values of $M_{\eta'}$ and $Q_{\eta'}$, M^f, Q^f are the fitted values for each event, and we are using the primed values in the Dalitz plot. The nearly uniform population of points on the plot is characteristic of $J^{PC}=0^{-+}$ (but such a distribution can also be approximated by a suitable mixture of $J^{PC}=2^{-+}$ matrix elements). The results of the fits to $\eta'\to\pi^+\pi^-\eta_N$ are given in Table V. From this table it is seen that all quantum-number choices are excluded (confidence level less than 10^{-6}) except $J^{PC}=0^{-+}$ and a mixture of the two possible matrix elements characteristic of $J^{PC}=2^{-+}$. Spin 0 is slightly favored over spin 2. These results are illustrated in Fig. 21, which shows the distribution of $M(\pi^+\pi^-)$ [Fig. 21(a)] and of the cosine between the π^+ and the η in the $\pi\pi$ rest frame [Fig. 21(b)]. The solid curves in these figures are the predictions of the $J^{PC}=0^{-+}$ matrix element. The dashed line is the $M(\pi^+\pi^-)$ prediction of the best $J^{PC}=2^{-+}$ mixture. We note from Figs. 4(b)

TABLE VI. $\eta'\to\pi^+\pi^-\eta_C$.

Matrix element	Conf. level [a]
$C=+$, $J^P=0^-$	0.23
$M(0^-)(1+\alpha Y)\to\alpha=-0.10\pm0.07$	
$J^P=1^+$	Excluded
$J^P=1^-$	Excluded
$J^P=2^+$	Excluded
$J^P=2^-$, $l_\eta=2$	Excluded
$J^P=2^-$, $l_\eta=0$	Excluded
$J^P=2^-$ mixture: $M(l_\eta=0)+aM(l_\eta=2)$	
$a=(-0.05\pm0.10)+(0.34\pm0.04)i$	0.06
a(real) $=0.33^{+0.08}_{-0.06}$	1.6×10^{-3}
$C=-$, $J^P=0^-$	Excluded
$J^P=1^+$	8×10^{-5}
$J^P=1^-$	Excluded
$J^P=2^+$	Excluded
$J^P=2^-$	3×10^{-3}

[a] Excluded means conf. level less than 10^{-6}.

TABLE VII. $\eta'\to\pi^+\pi^-\eta_N$ and $\pi^+\pi^-\eta_C$.

Matrix element	Conf. level [a]
$C=+$, $J^P=0^-$	0.11
$M(0^-)(1+\alpha Y)\to\alpha=-0.05\pm0.03$	
$J^P=1^+$	Excluded
$J^P=1^-$	Excluded
$J^P=2^+$	Excluded
$J^P=2^-$, $l_\eta=2$	Excluded
$J^P=2^-$, $l_\eta=0$	Excluded
$J^P=2^-$ mixture: $M(l_\eta=0)+aM(l_\eta=2)$	
$a=-0.02\pm0.05+(0.35\pm0.02)i$	0.03
a(real)	Excluded
$C=-$, $J^P=0^-$	Excluded
$J^P=1^+$	Excluded
$J^P=1^-$	Excluded
$J^P=2^+$	Excluded
$J^P=2^-$	Excluded

[a] Excluded means conf. level less than 10^{-6}.

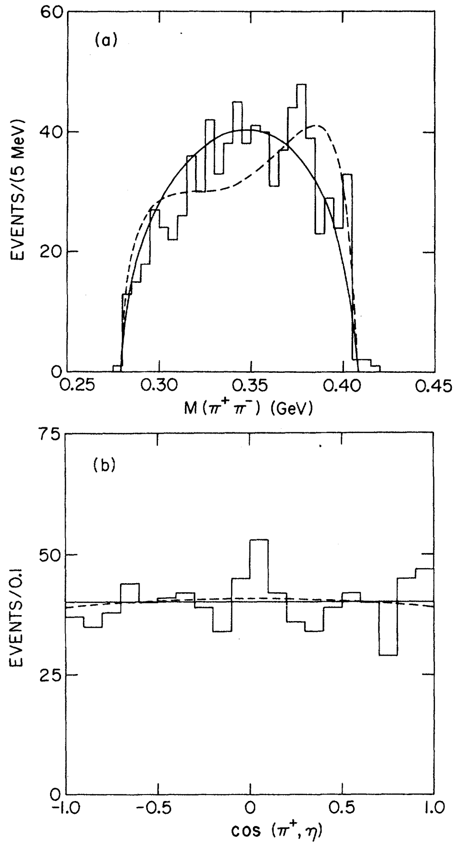

FIG. 24. (a) $M(\pi^+\pi^-)$ projection and (b) cosine (π^+,η). These data are the combined data of Figs. 20–23 for which the matrix elements have been refitted. The solid curve represents the $J^P = 0^-$ fit, and the dashed curve the best $J^P = 2^-$ fit.

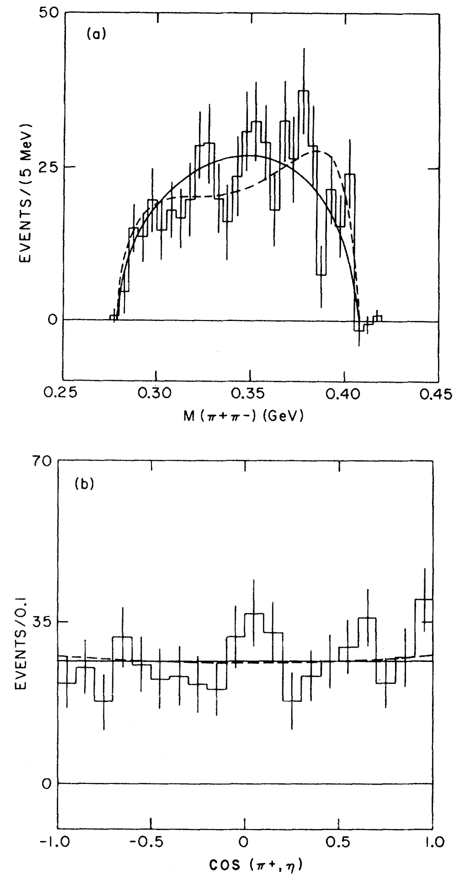

FIG. 25. (a) $M(\pi^+\pi^-)$ projection and (b) cosine (π^+,η). These data are the subtracted data of Fig. 24 (see text). The solid curve represents the $J^P = 0^-$ fit, and the dashed curve the best $J^P = 2^-$ fit.

and 4(c) that the $\eta' \to \pi^0\pi^0\eta_C$ contamination of the $\eta' \to \pi^+\pi^-\eta_N$ events is not expected to distort appreciably the distribution of events in the $\eta' \to \pi^+\pi^-\eta_N$ Dalitz plot.

The Dalitz plot for $\eta' \to \pi^+\pi^-\eta_C$ events (normalized, as the $\eta' \to \pi^+\pi^-\eta_N$ events were, to an η' mass of 958 MeV) is shown in Fig. 22. There are 179 events in this plot, about 15% of which are estimated to be background. Again the distribution of points appears nearly uniform. The fit results are displayed in Table VI, where $J^{PC} = 0^{-+}$ is favored over $J^{PC} = 2^{-+}$ as in the previous case. The Dalitz plot projections for $\eta' \to \pi^+\pi^-\eta_C$ are shown in Fig. 23; as before the solid curves are the predictions of a $J^{PC} = 0^{-+}$ matrix element, and the dashed curves are the predictions of the best $J^{PC} = 2^{-+}$ fit.

Since the $\eta' \to \pi^+\pi^-\eta_N$ and the $\eta' \to \pi^+\pi^-\eta_C$ results are consistent with each other, we have also combined these samples and performed the fits again. The results are given in Table VII. In the combined sample, $J^P = 0^-$ is favored by a factor of about 4 in confidence level over $J^P = 2^-$. Figure 24 displays the results of the $J^{PC} = 0^{-+}$ fit (solid curves) and of the $J^{PC} = 2^{-+}$ mixture (dashed curve).

Finally, since there is some background and since there are misidentified $\pi^0\pi^0\eta_C$ events in the combined $\eta' \to \pi^+\pi^-\eta_N$ and $\eta' \to \pi^+\pi^-\eta_C$ sample, we have performed a subtraction on the $M(\pi^+\pi^-)$ and $\cos\theta(\pi^+\eta)$ distributions. The distributions of events in the $M(\pi^+\pi^-\eta)$ intervals (937, 947 MeV) and (970, 980 MeV) are subtracted from the central region (947, 970 MeV). These side-band intervals are estimated to contain the same amount of background as the central region. In addition the distributions due to 51 $\pi^0\pi^0\eta_C$ events are subtracted. These distributions were discussed earlier and are shown in Figs. 4(b) and 4(c). The subtracted distributions with errors are shown in Fig. 25. Fits of the matrix elements again were made to those distributions. The results of these fits are given in Table VIII, and the spin-0 and -2 fits are shown as curves on the data of Fig. 25. Spin 0 is favored over spin 2 by about a factor of 5 in confidence level. For a spin-0 assignment, the linear

TABLE VIII. Subtracted $\eta' \to \pi^+\pi^-\eta_N$ and $\pi^+\pi^-\eta_C$.

Matrix element	Conf. level [a]
$C=+$, $J^P=0^-$	0.14
$M(0^-)(1+\alpha Y) \to \alpha = 0 \pm 0.10$	
$J^P=1^+$	Excluded
$J^P=1^-$	Excluded
$J^P=2^+$	Excluded
$J^P=2^-$, $l_\eta=2$	Excluded
$J^P=2^-$, $l_\eta=0$	Excluded
$J^P=2^-$ mixture: $M(l_\eta=0)+aM(l_\eta=2)$	
$a=(0.02\pm0.07)+(0.35\pm0.02)i$	0.03
a(real) $=0.34\pm0.02$	3.2×10^{-4}
$J^P=2^-$, $l_\eta=2$ with $\epsilon(M,\Gamma)=(750$ MeV, $100\to500$ MeV)	Excluded
$l_\eta=0$ with $f(M,\Gamma)=(1270$ MeV, 156 MeV)	Excluded
$J^P=2^-$, $M(l_\eta=0)\times \mathrm{BW}_f(1270,156)+aM(l_\eta=2)\times \mathrm{BW}_\epsilon(750,100)$	0.06 [b]
$J^P=2^-$, $M(l_\eta=0)\times \mathrm{BW}_f(1270,156)+aM(l_\eta=2)\times \mathrm{BW}_\epsilon(750,\Gamma_\epsilon)$	0.06 [c]
$J^P=2^-$, $M(l_\eta=0)+(\mathrm{Re}\,a)M(l_\eta=2)+(\mathrm{Im}\,b)M(l_\eta=l_{\pi\pi}=2)$	0.26 [d]
$C=-$, $J^P=0^-$	Excluded
$J^P=1^+$	Excluded
$J^P=1^-$	Excluded
$J^P=2^+$	Excluded
$J^P=2^-$	3.6×10^{-5}

[a] Excluded means conf. level less than 10^{-6}.
[b] $a=(0.01\pm0.06)+(0.29\pm0.02)i$.
[c] $\Gamma_\epsilon=(43\pm18)$ MeV and $a=(0.07\pm0.14)+(0.66\pm0.28)i$.
[d] $a=(-0.35\pm0.03)$ and $b=(0.52\pm0.12)i$.

matrix-element parameter α is now zero, although with a larger error.

Since, as it will be shown below, an assignment of $J^P=2^-$ for the η' may be indicated from a consideration of production and decay angular correlations, additional 2^- matrix-element fits (given in Table IV) were performed on the subtracted data of Fig. 25. One fit included a $(l_{\pi\pi}=2,\ l_\eta=2)$ matrix element for $C=+1$ orthogonal to the usual two terms for $J^P=2^-$ which were taken as relatively real.[13] A good fit was obtained, although the magnitude of the $(l_{\pi\pi}=2,\ l_\eta=2)$ contribution may be excessive. The other fit allowed ϵ^0 and/or f^0 Breit-Wigner distributions in the $C=+1$ matrix elements; no substantial improvement was obtained, however.

From these $\pi\pi\eta$ Dalitz-plot projection results we conclude that spin 0 is a more likely assignment for the η' than spin 2.

TABLE IX. Matrix elements M for $\eta'\to\pi^+\pi^-\gamma$. m is the $\pi\pi$ invariant mass. $\vec{k}$ is the photon momentum, $\vec{q}=\frac{1}{2}(\vec{p}_{\pi^+}-\vec{p}_{\pi^-})$, and θ is the angle between the π^+ and the γ directions, all in the $\pi\pi$ rest frame. $|M|^2$ is summed over spins.

Quantum numbers	$l_{\pi\pi}$	Multipole	$\lvert M\rvert^2$
$C=+$, $J^P=0^\pm$	1	dipole	$q^2k^2m^2\sin^2\theta$
$J^P=1^\pm$	1	dipole	$q^2k^2[1+\cos^2\theta-(2km/m_{\eta'}{}^2)\sin^2\theta]$
$J^P=1^\pm$	1	quadrupole	$(q^2k^4m^4/m_{\eta'}{}^2)\sin^2\theta$
$J^P=2^\pm$	1	dipole	$q^2k^2m^2[6+\sin^2\theta+6(k/m_{\eta'})^2\cos^2\theta]$
$J^P=2^\pm$	1	octupole	$(q^2k^6m^6/m_{\eta'}{}^4)\sin^2\theta$
$J^P=2^\pm$ mixture	1	dipole + quadrupole	$q^2k^2m^2[6+\sin^2\theta+6(k/m_{\eta'})^2\cos^2\theta]$ $-4(\mathrm{Re}\,a)(q^2k^3m^2/m_{\eta'})$ $\times[1+2\cos^2\theta-(km/m_{\eta'}{}^2)(2+\cos^2\theta)]$ $+2\lvert a\rvert^2(q^2k^4m^2/m_{\eta'}{}^2)[2+\cos^2\theta-4(km/m_{\eta'}{}^2)\sin^2\theta]$
$C=-$, $J^P=0^\pm$	2	quadrupole	$q^4k^4m^2\sin^2\theta\cos^2\theta$
$J^P=1^\pm$	0	dipole	k^2m^2
$J^P=2^\pm$	2	dipole	$q^4k^4\{1+\cos^2\theta+(2km/m_{\eta'}{}^2)$ $\times[(2km/3m_{\eta'}{}^2)\cos^2\theta-\sin^2\theta]$ $+(2k^2/3m_{\eta'}{}^2)[1+(4km/m_{\eta'}{}^2)]\cos^4\theta\}$
$J^P=2^\pm$	0	quadrupole	$k^4m^4/m_{\eta'}{}^2$

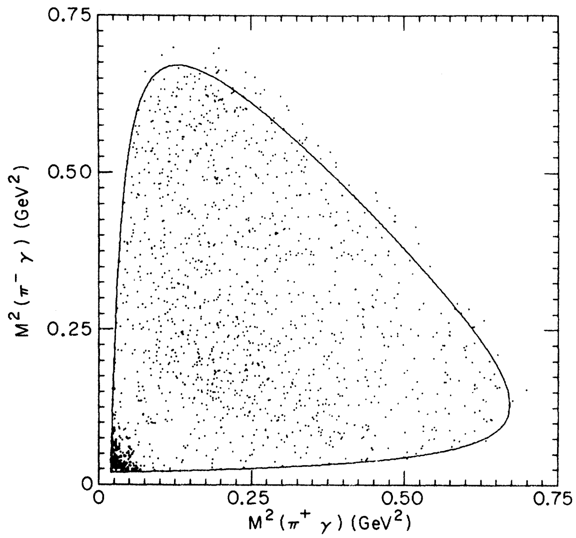

FIG. 26. Dalitz plot of $M^2(\pi^+\gamma)$ vs $M^2(\pi^-\gamma)$ for $\Lambda\pi^+\pi^-\gamma$ events in the η' region.

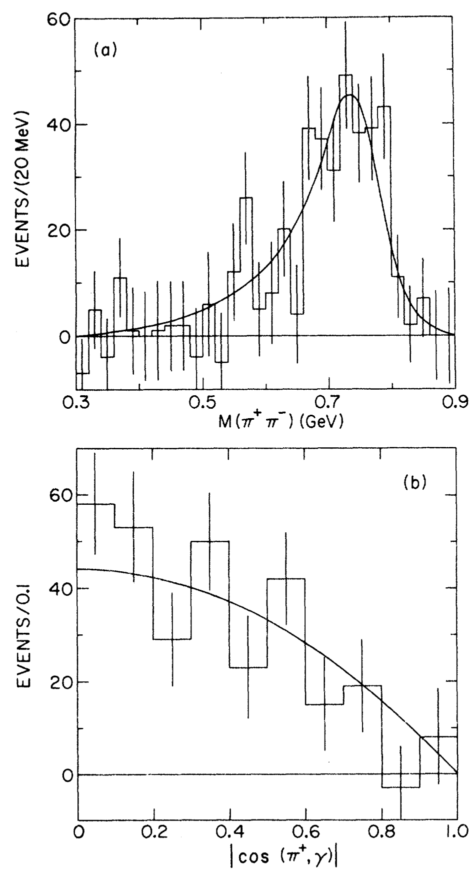

FIG. 27. Projections of Dalitz plot of Fig. 26 after subtraction of side bands (see text). (a) $M(\pi^+\pi^-)$ projection, and (b) cosine (π^+, γ) projection for ρ band [620 $< M(\pi^+\pi^-) <$ 880 MeV]. The curves represent the $J^P = 0^-$ fit.

The electromagnetic decay $\eta' \to \pi^+\pi^-\gamma$ can be characterized by the multipole order of the transition. Table IX gives the predicted distributions[3] for spins 0, 1, 2. The Dalitz plot for events in the η' band, $M(\pi^+\pi^-\gamma) = (960 \pm 30)$ MeV, is shown in Fig. 26. The plot boundary corresponds to an η' mass of 960 MeV. Some two-thirds of the events in this plot are estimated to be background events, and ignoring the cluster of points in the corner of the plot due to $\Lambda\pi^+\pi^-$ events not excluded by the selection procedure, there appears to be a diagonal band of higher intensity superimposed upon a uniform background distribution. To get the true distribution of $M(\pi^+\pi^-)$, we subtract from the η'-band $M(\pi^+\pi^-)$ distribution the distribution of events in the $M(\pi^+\pi^-\gamma)$ side bands adjacent to the η' band. The side bands are the $M(\pi^+\pi^-\gamma)$ intervals (900, 930 MeV) and (990, 1020 MeV). The results of this subtraction are shown in Fig. 27(a). It is seen that the $M(\pi^+\pi^-)$ spectrum can be accounted for entirely as $\rho \to \pi^+\pi^-$ (or possibly $\epsilon^0 \to \pi^+\pi^-$). In order to get a sample with even less background on which to perform fits to the cosine of the angle between the π^+ and the γ in the $\pi\pi$ rest frame, the background subtraction procedure was repeated for events in the ρ band of $M(\pi^+\pi^-)$ [$M(\pi^+\pi^-) = (750 \pm 130)$ MeV]. The resulting cosine distribution is given in Fig. 27(b). The matrix elements of Table IX were fitted to the distributions of Fig. 27; the results are listed in Table X. The best fit was obtained for spin 0; the results of this fit are the curves in Fig. 27. Note that this fit de-

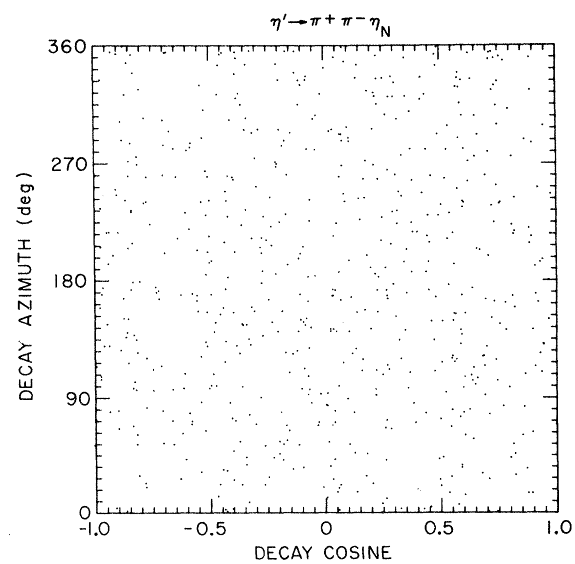

FIG. 28. Production-decay angular correlations for $\Lambda\pi^+\pi^-\eta_N$ events in the η' region with $-t < 0.7$ GeV^2; scatter plot of decay cosine vs decay azimuth in the Jackson frame.

TABLE X. $\eta' \to \pi^+\pi^-\gamma$.

Matrix element	Conf. level [a]
$C=+$, $J^P=0^\pm$, dipole transition	Excluded
$J^P=0^\pm$, dipole transition, ρ resonance	0.66
$J^P=1^\pm$, dipole transition	Excluded
$J^P=1^\pm$, dipole transition, ρ resonance	Excluded
$J^P=1^\pm$, quadrupole transition, ρ resonance	0.03 [b]
$J^P=2^\pm$, dipole transition	Excluded
$J^P=2^\pm$, dipole transition, ρ resonance	0.02
$J^P=2^\pm$, quadrupole, ρ resonance	Excluded
$J^P=2^\pm$, octupole transition, ρ resonance	Excluded
$J^P=2^\pm$, dipole + quadrupole, ρ resonance	
$a=(2.4\pm0.5)+(0\pm0.6)i$	0.26 [c]
$C=-$, $J^P=0^\pm$, quadrupole transition	Excluded
$J^P=1^\pm$	Excluded
$J^P=1^\pm$, dipole, ϵ^0 resonance $(M,\Gamma)=(765\text{ MeV}, 125\text{ MeV})$	6×10^{-4}
$J^P=2^\pm$, dipole transition	Excluded
$J^P=2^\pm$, quadrupole	Excluded
$J^P=2^\pm$, quadrupole, ϵ^0 resonance $(M,\Gamma)=(765\text{ MeV}, 125\text{ MeV})$	Excluded
Fit to $\cos(\pi^+,\gamma)$ distribution only:	
$f(\theta)=a+\sin^2\theta \Rightarrow a=0^{+0.3}_{-0}$	0.24 [d]

[a] Excluded means conf. level less than 10^{-6}.
[b] A mixture of dipole + quadrupole will also fit.
[c] $f(\theta)\simeq 0.6+\sin^2\theta$.
[d] Conf. level = 0.002 for $f(\theta)=1.48+\sin^2\theta$ (see Ref. 13).

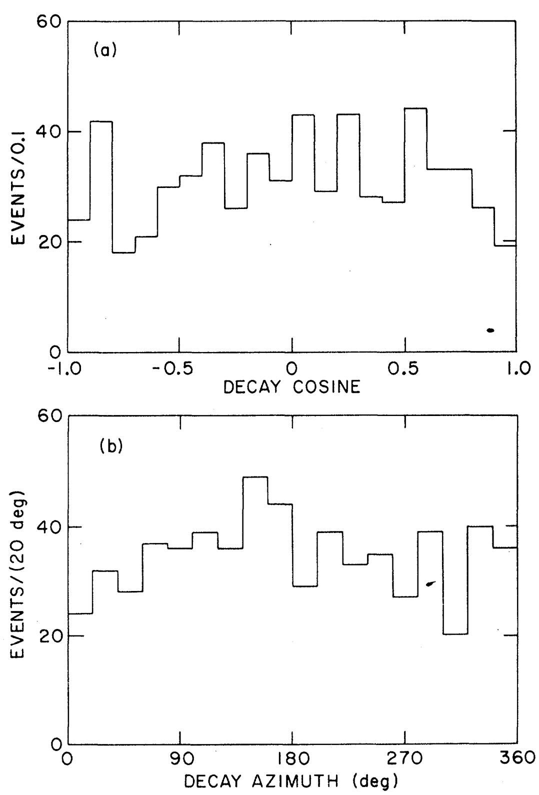

FIG. 29. Projections of Fig. 28: (a) decay cosine, and (b) decay azimuth.

scribes the $M(\pi^+\pi^-)$ spectrum with a ρ-resonance line shape.

We have also fitted the cosine distribution of Fig. 27(b) to the functional form

$$f(\theta)=a+\sin^2\theta;$$

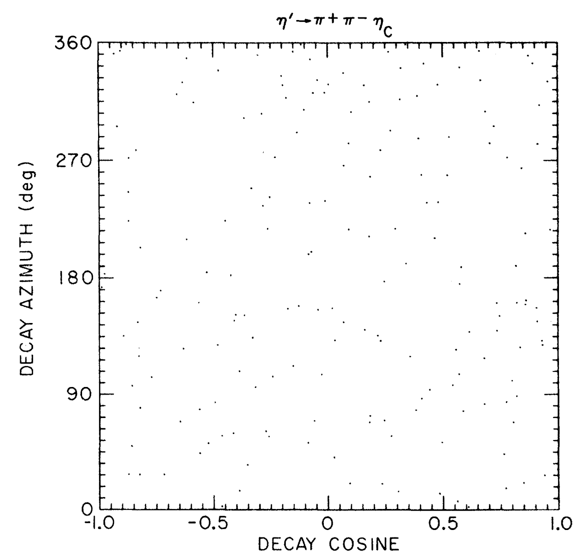

FIG. 30. Production-decay angular correlations for $\Lambda\pi^+\pi^-\eta_C$ events in the η' region with $-t < 0.7\text{ GeV}^2$; scatter plot of decay cosine vs decay azimuth in the Jackson frame.

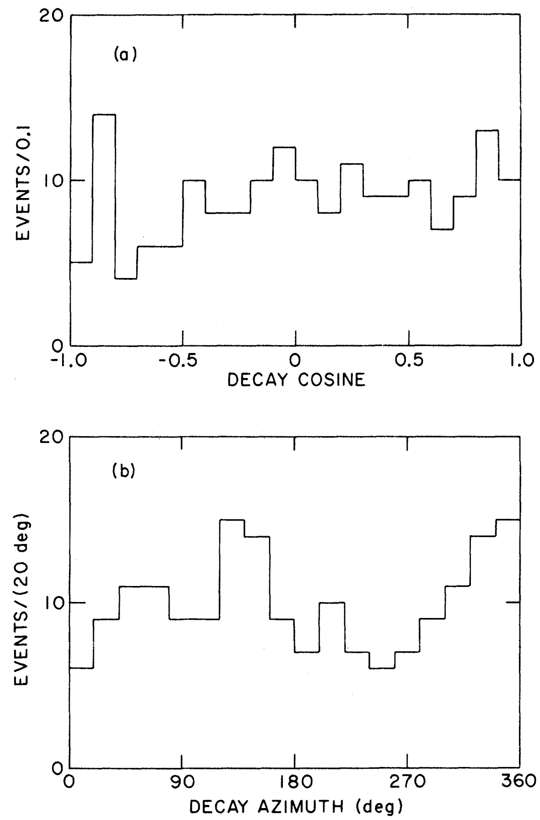

FIG. 31. Projections of Fig. 30: (a) decay cosine, and (b) decay azimuth.

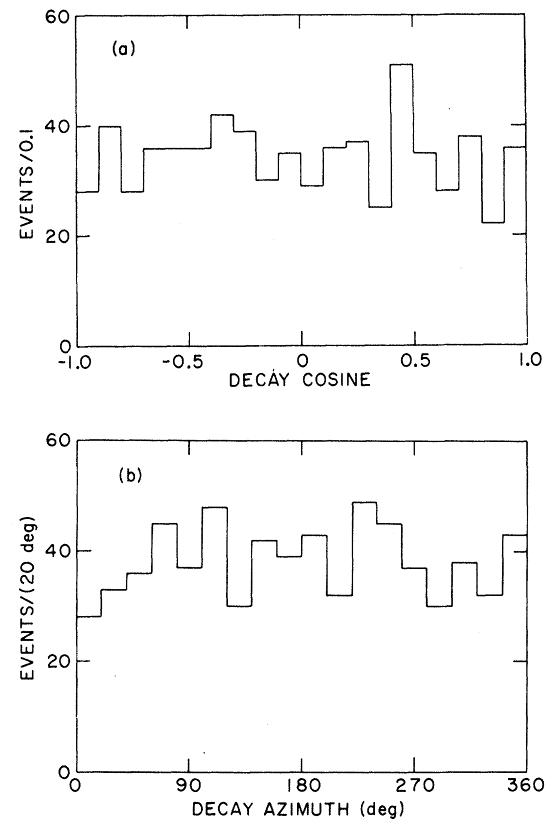

FIG. 33. Projections of Fig. 32: (a) decay cosine, and (b) decay azimuth.

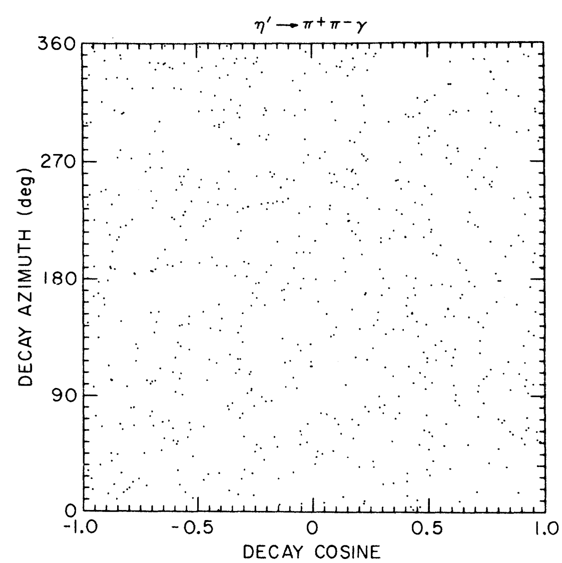

FIG. 32. Production-decay angular correlations for $\Lambda\pi^+\pi^-\gamma$ events in the η' region with $-t < 0.7$ GeV^2; scatter plot of decay cosine vs decay azimuth in the Jackson frame.

we find $a=0^{+0.3}_{-0}$. This excludes a prediction[13] of $a=1.48$ for a spin-2 η'.

We have fitted additional $C=-1$ matrix elements for the purpose of excluding an s-wave $\pi^+\pi^-$ resonance near the ρ-meson mass as an explanation of the $\pi^+\pi^-\gamma$ Dalitz plot. The fits are rejected.

Although the combined results of all these Dalitz-plot fits to the $\eta' \to \pi^+\pi^-\eta$ and $\eta' \to \pi^+\pi^-\gamma$ matrix-element predictions favor $J^{PC}=0^{-+}$, we defer a conclusion until the considerations of Sec. IV B.

B. Decay Angular Distributions

The η' decay angular distributions do not yield conclusive evidence that the η' spin is indeed 0. To examine the η' decay angular distributions we work in the Jackson frame, which is the rest frame of the η', with the beam direction as the z axis (polar axis) and the production normal as the y axis. The η' decay direction is the direction of the normal to the decay plane of the three decay particles ($\pi\pi\eta$ or $\pi\pi\gamma$).

For $J^P=0^-$ the decay angular distributions of $\cos\theta$ (the decay cosine) and ϕ (the decay azimuth)

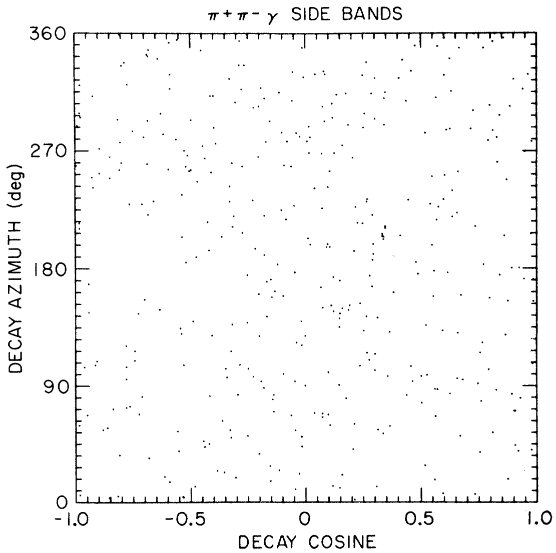

FIG. 34. Production-decay angular correlations for $\Lambda\pi^+\pi^-\gamma$ side-band events (see text) in the η' region with $-t<0.7$ GeV^2; scatter plot of decay cosine vs decay azimuth in the Jackson frame.

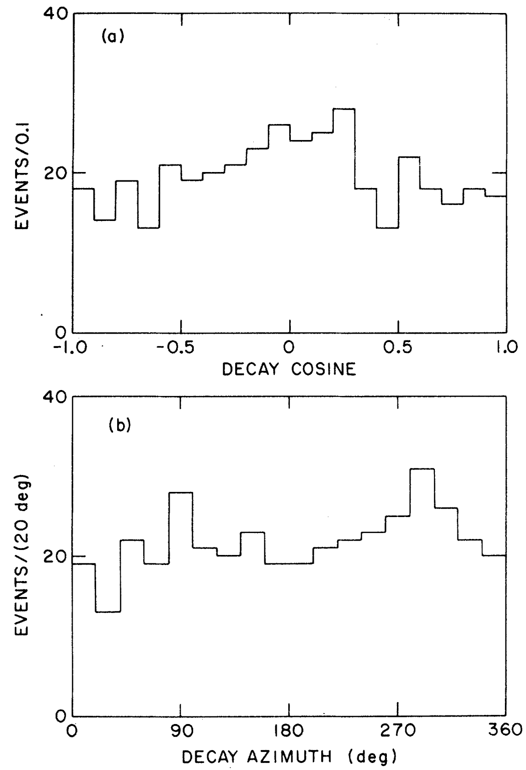

FIG. 35. Projections of Fig. 34: (a) decay cosine, and (b) decay azimuth.

must be isotropic. For $J^P=2^-$ it is conceivable that the angular distributions could be isotropic, but for nonzero-spin particles this is, in general, not the case. Figure 28 is a plot of $\cos\theta$ vs ϕ for $\eta'\to\pi^+\pi^-\eta_N$; Fig. 29 shows the projections of the scatter plot of Fig. 28. The consistency of the plots with isotropy is evident. The corresponding plots for $\eta'\to\pi^+\pi^-\eta_C$ are displayed in Figs. 30 and 31. Figures 32 and 33 show the same decay angular distributions for events in the η' band (930 –990 MeV) of the $M(\pi^+\pi^-\gamma)$ spectrum, and since there is considerable background in this signal region, the results for the η' side bands in $M(\pi^+\pi^-\gamma)$ (900–930 MeV and 990–1020 MeV) are shown in Figs. 34 and 35. The behavior of the events in the η' side bands is expected to be rep-

TABLE XI. Moments of decay angular distribution (Jackson frame), $\eta'\to\pi^+\pi^-\eta_N$.

(a) Moments of Re(Y_l^m)

$l\backslash m$	0	1	2	3	4	5
1	0.06±0.14	0.40±0.21				
2	−0.38±0.14	−0.18±0.20	0.12±0.21			
3	−0.26±0.13	0.23±0.20	0.08±0.20	−0.06±0.21		
4	−0.07±0.13	−0.05±0.20	−0.15±0.20	−0.32±0.20	0.03±0.21	
5	−0.20±0.13	0.25±0.20	0.12±0.20	−0.40±0.20	0.05±0.20	−0.17±0.21

(b) Moments of Im(Y_l^m)

$l\backslash m$	1	2	3	4	5
1	−0.20±0.20				
2	0.09±0.20	−0.26±0.21			
3	−0.05±0.20	−0.19±0.20	−0.04±0.21		
4	−0.17±0.19	−0.03±0.20	0.26±0.20	−0.22±0.21	
5	−0.09±0.19	0.09±0.20	0.09±0.20	0.02±0.21	−0.10±0.21

TABLE XII. Moments of decay angular distribution (Jackson frame), $\eta' \to \pi^+\pi^-\eta_C$.

(a) Moments of $\mathrm{Re}(Y_l^m)$

$l \backslash m$	0	1	2	3	4	5
1	0.37 ± 0.26	−0.32 ± 0.38				
2	−0.11 ± 0.27	0.01 ± 0.37	0.09 ± 0.36			
3	0 ± 0.25	0.27 ± 0.40	−0.22 ± 0.37	0.02 ± 0.38		
4	0.10 ± 0.24	0.32 ± 0.40	0.08 ± 0.38	−0.26 ± 0.37	−0.64 ± 0.37	
5	−0.10 ± 0.25	0.07 ± 0.40	0.16 ± 0.39	0.01 ± 0.35	0.62 ± 0.37	−0.30 ± 0.39

(b) Moments of $\mathrm{Im}(Y_l^m)$

$l \backslash m$	1	2	3	4	5
1	−0.32 ± 0.37				
2	0.12 ± 0.37	−0.82 ± 0.39			
3	−0.66 ± 0.37	−0.43 ± 0.36	0.45 ± 0.38		
4	−0.34 ± 0.38	−0.17 ± 0.38	0.11 ± 0.36	−0.79 ± 0.39	
5	0.41 ± 0.35	−0.45 ± 0.39	−0.17 ± 0.38	0.27 ± 0.36	0.21 ± 0.38

resentative of that of the background events in the η' band. All the decay angular distributions in Figs. 28–35 appear to be consistent with isotropy, when summed over all momentum transfers $-t$ less than 0.7 GeV^2.

This isotropy of all the distributions shown was confirmed by calculating the moments of the real and imaginary parts of the spherical harmonics $Y_l^m(\theta, \phi)$. Tables **XI–XIV** show the results of the moments calculations for all four data samples described above, for $l=1$ through 5. From these tables no pattern of nonzero moments emerges. Of the total of 140 moments calculated, 11 are of more than two standard deviations significance, compared to about 7 expected to have this significance in a random sample.

From these results in the η' decay angular distributions we conclude that all decay distributions (averaged over all t) are compatible with isotropy. However, a closer examination of the decay angular distributions for various t cuts shows possible deviations from isotropy. Ogievetsky, Tybor, and Zaslavsky,[13] proponents for a $J^P=2^-$ η' meson, have emphasized that the production-decay corre-

TABLE XIII. Moments of decay angular distribution (Jackson frame), $\eta' \to \pi^+\pi^-\gamma$ (signal band).

(a) Moments of $\mathrm{Re}(Y_l^m)$

$l \backslash m$	0	1	2	3	4	5
1	−0.04 ± 0.13	0.29 ± 0.19				
2	−0.13 ± 0.13	0.27 ± 0.19	−0.23 ± 0.19			
3	0.02 ± 0.14	0.01 ± 0.19	−0.13 ± 0.19	−0.17 ± 0.20		
4	−0.08 ± 0.13	−0.12 ± 0.19	−0.02 ± 0.19	0.25 ± 0.20	0 ± 0.19	
5	0.09 ± 0.13	−0.09 ± 0.19	−0.28 ± 0.19	−0.04 ± 0.19	0.06 ± 0.19	0.13 ± 0.19

(b) Moments of $\mathrm{Im}(Y_l^m)$

$l \backslash m$	1	2	3	4	5
1	0.06 ± 0.20				
2	−0.08 ± 0.19	0.08 ± 0.19			
3	−0.33 ± 0.19	−0.21 ± 0.19	0.07 ± 0.19		
4	−0.07 ± 0.19	−0.10 ± 0.18	−0.24 ± 0.19	−0.41 ± 0.19	
5	−0.01 ± 0.19	−0.27 ± 0.19	0.19 ± 0.19	0.18 ± 0.20	0.06 ± 0.20

TABLE XIV. Moments of decay angular distribution (Jackson frame), $\pi^+\pi^-\gamma$ side bands.

(a) Moments of $\mathrm{Re}(Y_l^m)$

$l \backslash m$	0	1	2	3	4	5
1	0.04 ± 0.17	0.10 ± 0.25				
2	-0.45 ± 0.18	0.35 ± 0.23	-0.40 ± 0.26			
3	-0.04 ± 0.17	-0.50 ± 0.23	0.34 ± 0.25	0.35 ± 0.26		
4	0.33 ± 0.18	-0.23 ± 0.23	-0.26 ± 0.26	0.25 ± 0.24	-0.11 ± 0.27	
5	-0.07 ± 0.18	0.15 ± 0.23	0.07 ± 0.25	-0.66 ± 0.25	-0.09 ± 0.26	-0.28 ± 0.27

(b) Moments of $\mathrm{Im}(Y_l^m)$

$l \backslash m$	1	2	3	4	5
1	0.32 ± 0.27				
2	-0.28 ± 0.25	-0.31 ± 0.27			
3	0.04 ± 0.26	-0.22 ± 0.24	0.17 ± 0.28		
4	-0.05 ± 0.26	0.11 ± 0.24	0.59 ± 0.25	0.10 ± 0.27	
5	-0.11 ± 0.26	0.16 ± 0.24	0.21 ± 0.25	0.04 ± 0.24	-0.16 ± 0.28

lations should be studied for η' mesons produced in the extreme forward direction. They and Klosinski, Rembielinski, and Tybor[14] point out that production-decay correlations must exist for the very forward η', if indeed $J^P = 2^-$.

For the $\pi^+\pi^-\eta$ decay mode, the distributions of the decay plane normal $\hat{n}$ and of the $\eta(549)$, $\hat{\eta}$, with respect to the incident beam $\hat{K}$ were calculated in the η' rest frame. For the $\rho^0\gamma$ decay, the gamma direction $\hat{\gamma}$ relative to the beam $\hat{K}$ was used. The distributions $(\hat{n} \cdot \hat{K})$, $(\hat{\eta} \cdot \hat{K})$, and $(\hat{\gamma} \cdot \hat{K})$ are each presented as a polar-equatorial ratio P/E due to the severe statistical limitation imposed by the "very forward" cut. The P/E ratios are presented in Table XV and Fig. 36 for various production angle cuts on $\cos\theta^* = (\hat{K} \cdot \hat{\eta}')$ in the K^-p c.m. system. Isotropic distributions are characterized by $P/E = 1$. Anisotropies should appear for events with $\cos\theta^*$ near 1 if $J = 2$. The standard prescription that $\theta^* < (kr)^{-1}$ implies $\langle\theta^*\rangle \simeq 0.1$, so $\theta^* < 0.2$ rad should suffice,[14] i.e., $\cos\theta^* > 0.98$. However, only 7% of all data survive such a cut (93 events in both decay modes). The P/E ratios for $\cos\theta^* > 0.98$ in the data are $P/E(\hat{n} \cdot \hat{K}) = 0.54 \pm 0.14$ and $P/E(\hat{\gamma} \cdot \hat{K}) = 0.35 \pm 0.31$, both deviating from unity, and for $0.6 < \cos\theta^* < 0.98$, $P/E(\hat{n} \cdot \hat{K}) = 0.89 \pm 0.07$ and $P/E(\hat{\eta} \cdot \hat{K}) = 1.12 \pm 0.09$ also deviate from unity. These four numbers have a probability (in a χ^2 sense) of a few tenths of a percent to be in agreement with isotropy. The angular distributions for $\cos\theta^* > 0.98$ are presented in Fig. 37 with theoretical curves[14] for $\rho_{00} = 0.5$. These data give as much evidence for $J = 2$ as the Dalitz plots do for $J = 0$; that is, the confidence level for $J = 0$ is less than that for $J = 2$ from the production and decay correlations, whereas $J = 2$ is less probable than $J = 0$ from the Dalitz-plot analysis.

Several Monte Carlo studies were undertaken to verify that the observed asymmetries were not introduced into a 0^- η' decay by any known bias. No effects in the P/E ratios of greater than 1% were discovered. The following biases were elim-

TABLE XV. Polar-equatorial ratios (P/E) as a function of the c.m. production $\cos\theta^* = (\hat{K} \cdot \hat{\eta}')$ for the reaction $K^-p \to \Lambda\eta'(958)$. $\hat{n} \cdot \hat{K}$ is the cosine of the polar angle of the normal to the $\pi^+\pi^-\eta(548)$ decay plane relative to the incident K beam in the η' rest frame, $\hat{\eta} \cdot \hat{K}$ is that of the η, and $\hat{\gamma} \cdot \hat{K}$ is that of the γ in the $\eta' \to \rho^0\gamma$ decay. A background subtraction has been performed for the $\eta' \to \rho^0\gamma$ decays. The background region is 900–930 and 990–1020 MeV, respectively, and the η' region is 930–990 MeV. P is the number of events with $|\hat{n} \cdot \hat{K}|$ (or $|\hat{\eta} \cdot \hat{K}|$ or $|\hat{\gamma} \cdot \hat{K}|$) >0.5; E is the number of events with $|\hat{n} \cdot \hat{K}|$ (or $|\hat{\eta} \cdot \hat{K}|$ or $|\hat{\gamma} \cdot \hat{K}|$) <0.5.

	$\eta' \to \pi^+\pi^-\eta$		$\eta' \to \rho^0\gamma$
	$\frac{P}{E}(\hat{n} \cdot \hat{K})$	$\frac{P}{E}(\hat{\eta} \cdot \hat{K})$	$\frac{P}{E}(\hat{\gamma} \cdot \hat{K})$
$0.6 \leq \cos\theta^* < 0.8$	0.93 ± 0.14	1.17 ± 0.17	1.00 ± 0.43
$0.8 \leq \cos\theta^* < 0.9$	0.88 ± 0.12	1.15 ± 0.16	1.29 ± 0.63
$0.9 \leq \cos\theta^* \leq 1.0$	0.79 ± 0.09	1.12 ± 0.12	0.66 ± 0.21
$0.9 \leq \cos\theta^* < 0.96$	0.80 ± 0.12	1.12 ± 0.17	0.76 ± 0.33
$0.96 \leq \cos\theta^* \leq 1.0$	0.78 ± 0.13	1.12 ± 0.19	0.56 ± 0.26
$0.9 \leq \cos\theta^* < 0.94$	0.76 ± 0.14	1.15 ± 0.21	0.56 ± 0.34
$0.94 \leq \cos\theta^* < 0.98$	0.97 ± 0.16	0.97 ± 0.16	1.00 ± 0.44
$0.9 \leq \cos\theta^* < 0.98$	0.87 ± 0.11	1.05 ± 0.13	0.78 ± 0.27
$0.6 \leq \cos\theta^* < 0.98$	0.89 ± 0.07 [a]	1.12 ± 0.09	0.97 ± 0.23 [b]
$0.98 \leq \cos\theta^* \leq 1.0$	0.54 ± 0.14 [c]	1.44 ± 0.36	0.35 ± 0.31 [d]

[a] 311 polar and 349 equatorial events.

[b] $121 \pm (463)^{1/2}$ polar and $123 \pm (347)^{1/2}$ equatorial events.

[c] 23 polar and 43 equatorial events.

[d] $7 \pm (33)^{1/2}$ polar and $20 \pm (38)^{1/2}$ equatorial events.

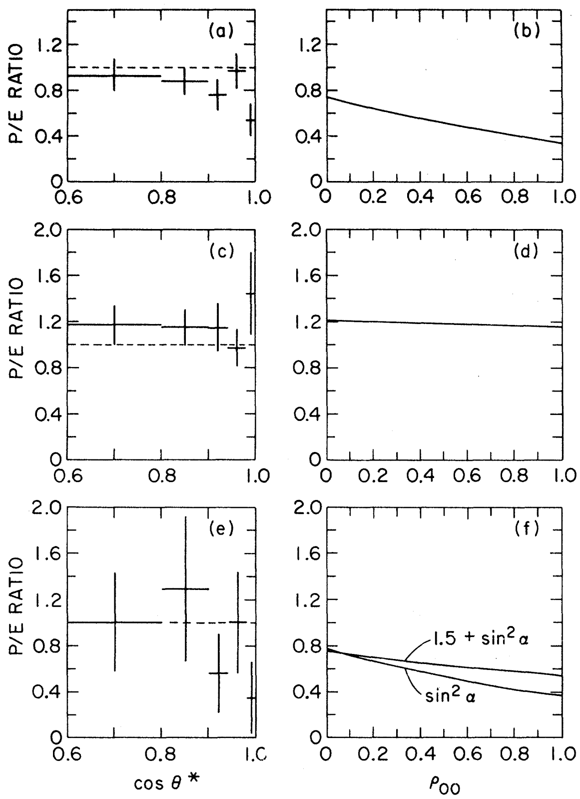

FIG. 36. Polar-equatorial, P/E, ratios of production and decay angular correlations for η' events (930–990 MeV) as a function of the production angular distribution $\cos\theta^*$ (see text); (a) $P/E(\hat{n}\cdot\hat{K})$ and (c) $P/E(\hat{\eta}\cdot\hat{K})$ for $\pi^+\pi^-\eta$ decays and (e) $P/E(\hat{\gamma}\cdot\hat{K})$ for $\pi^+\pi^-\gamma$ events with a side-band subtraction performed (see Table XV); and the predicted P/E ratios for extreme forward η' production ($\cos\theta^* \sim 1$) for the matrix elements of Klosinski, Rembielinski, and Tybor (see text and Ref. 14) as a function of the parameter ρ_{00} (b) for $P/E(\hat{n}\cdot\hat{K})$ and (d) $P/E(\hat{\eta}\cdot\hat{K})$ for $\pi^+\pi^-\eta$ decays, and (f) for $P/E(\hat{\gamma}\cdot\hat{K})$ for $\pi^+\pi^-\gamma$ decays. For $\pi^+\pi^-\eta$ the values of $B_0{:}B_1{:}B_2$ are 1:0:3.72 for $P/E(\hat{n}\cdot K)$ and 1:0.38:0.34 for $P/E(\hat{\eta}\cdot\hat{K})$; for $\pi^+\pi^-\gamma$ the values of $C_0{:}C_1{:}C_2$ are 1:−0.34:1 for the curve labeled $1.5+\sin^2\alpha$ and 1:−0.5:1 for the curve labeled $\sin^2\alpha$, where $\cos\alpha$ is the Dalitz-plot angle of Fig. 27(b).

inated as possible causes of the observed asymmetry:

(1) a systematic shift in the beam momentum leading to a fore/aft shift of the neutral momentum (η or γ) in fitting;

(2) a smaller than realistic beam-momentum error in fitting leading to a fore/aft shift of the neutral momentum in fitting (this effect is observable as a depletion of the very polar normals but results in few normals crossing the polar-equatorial boundary);

(3) a loss of events with a high-momentum track near zero degrees relative to the beam (the data

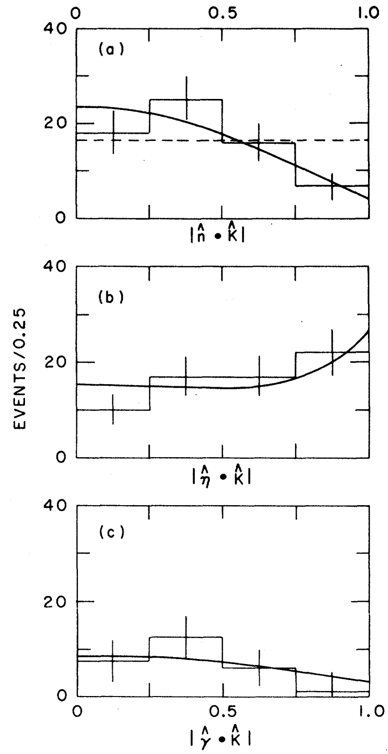

FIG. 37. The production and decay correlation distributions for $\cos\theta^* > 0.98$ (see text). (a) $|\hat{n}\cdot\hat{K}|$ for $\eta' \to \pi^+\pi^-\eta$; (b) $|\hat{\eta}\cdot\hat{K}|$ for $\eta' \to \pi^+\pi^-\eta$; and (c) $|\hat{\gamma}\cdot\hat{K}|$ for $\eta' \to \rho^0\gamma$ with background subtracted. The solid curves are the predictions of Ref. 14 for an arbitrary "m' ' lle" value of $\rho_{00}=0.5$; for $(\pi^+\pi^-\eta)$ $B_0{:}B_1{:}B_2 = 1{:}0{:}3.72$ $(\hat{n}\cdot\hat{K})$ and 1:0.38:0.34 $(\hat{\eta}\cdot\hat{K})$, and for $(\rho^0\gamma)$ $C_1{:}C_2{:}C_3 = 1{:}-0.5{:}1$ (a $\sin^2\alpha$ decay distribution).

were measured on a flying-spot scanner for which overlaying beam-track confusion could lead to an event loss);

(4) confusion as to whether the $\pi^+\pi^-$ selected as the primary decay products of the η' are actually from the subsequent decay of the η (misassignment of this type is small for the $\pi^+\pi^-\eta_N$ decay due to the favorable decay branching ratios involved; for the $\pi^+\pi^-\eta_C$ the misassignment is greater but no asymmetry results from misassigned events).

Thus the decay angular distributions for the very-forward-produced η' are anisotropic, suggesting that possibly $J^P = 2^-$ rather than 0^-. The previous large sample of 800 η' of Rittenberg[3] (LBL), however, does not give additioı ıl support for this possibility; the combined BNL-Michigan plus LBL data are reported elsewhere.[15] Thus $J^P = 0^-$ or 2^- are both tenable for the $\eta'(958)$ meson.

V. PRODUCTION ANGULAR DISTRIBUTIONS

We present in Fig. 38 for completeness the t distributions (with production cosine scales) for the reaction $K^-p \to \Lambda\eta'$, with η' decaying into $\pi^+\pi^-\eta_N$ [Fig. 38(a)], $\pi^+\pi^-\eta_C$ [Fig. 38(b)], $\pi^+\pi^-\gamma$ [Fig. 38(c)], and neutrals [Fig. 38(d)]. Parts (c) and (d) of the figure show background-subtracted distributions, since the signals presented there appear atop considerable background (cf. Figs. 10 and 13). The well-known peripheral peaking of these production distributions[3] is evident in this figure.

VI. CONCLUSIONS

We have observed $K^-p \to \Lambda\eta'$, η' decaying to $\pi^+\pi^-\eta_N$, $\pi^+\pi^-\eta_C$, $\pi^+\pi^-\gamma$, and all neutrals. The masses and widths of all modes are consistent. The J^P values of $\pi^+\pi^-\eta$ and $\rho^0\gamma$ are consistent with 0^- or 2^-. The momentum-transfer distributions of the various samples are the same. The decay branching ratios require nothing besides $\pi\pi\eta$, $\rho\gamma$, and $\gamma\gamma$. The energy dependence of the $(\rho\gamma/\pi\pi\eta)$ branching ratio from other data[2-7] is consistent with a constant value, although the errors are large. Thus we have no evidence for production of any other state in the mass region 930–980 MeV except the η', i.e., $K^-p \to \Lambda\eta'(958)$. Other possible states in this mass region, $M^0(940)$,[16] $M^0(953)$,[17] $\xi^0(953)$,[18] $\delta^0(963)$,[16,19-21] or $\pi_N(976)$,[21-23] are not observed in the reaction $K^-p \to \Lambda X^0$ at 2.18 GeV/c. We note that other than $\eta'(958)$, only the $\pi_N(976)$ state has substantial support as a reasonably well-established meson.[9,21-23]

We conclude that most of the η' properties are reasonably well established except for the possibility that $J^P = 2^-$ and except that the SU_3 character (presumably mostly singlet if $J^P = 0^-$) has not been directly demonstrated. Although some aspects of our data suggest that possibly $J^P = 2^-$, we should not revise our present assignment of $J^P = 0^-$ unless further anisotropies in the very-forward production and decay correlations are observed in future experiments, or unless some compelling theoretical reason is put forward.

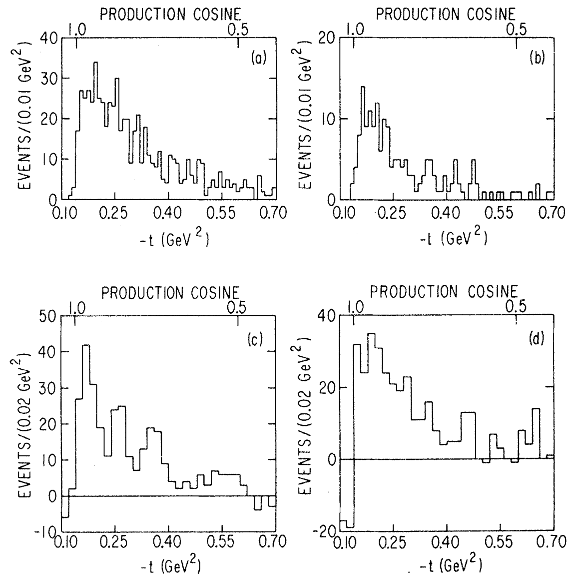

FIG. 38. The four-momentum transfer, $-t$, distributions of the η'-region events for (a) $\Lambda\pi^+\pi^-\eta_N$ events, (b) $\Lambda\pi^+\pi^-\eta_C$ events, (c) $\Lambda\pi^+\pi^-\gamma$ events, and (d) Λ + neutrals. For (c) and (d) the side-band region distributions have been subtracted. Note the similarity of all the distributions; this is expected if the events represent the various decay modes of the same meson, the η'.

ACKNOWLEDGMENTS

We thank Professor B. Roe, Dr. N. P. Samios, and Dr. R. P. Shutt for their support and encouragement.

*Work supported by the U. S. Atomic Energy Commission.

†Present address: Geophysics Department, Shell Development Company, Houston, Texas 77001.

‡Permanent address: York College, City University of New York, Queens, N. Y.

§Present address: 370 First Avenue, New York, New York 10010.

‖Present address: Flat 221, Avoca Street, Randwick, N. S. W. 2031, Australia.

[1]G. R Kalbfleisch *et al.*, Phys. Rev. Lett. 12, 527 (1964); 13, 349 (1964); M. Goldberg *et al.*, *ibid.* 12, 546 (1964); 13, 249 (1964).

[2]P. M. Dauber *et al.*, Phys. Rev. Lett. 13, 449 (1964).

[3]A. Rittenberg, UCRL Report No. UCRL-18863, 1969 (Ph.D. thesis, unpublished).

[4]A. Rittenberg and G. R. Kalbfleisch, Phys. Rev. Lett. 15, 556 (1965); G. W London *et al.*, Phys. Rev. 143, 1034 (1966); M. Aguilar-Benitez *et al.*, Phys. Rev. D 6, 29 (1972); S. M. Jacobs *et al.*, *ibid.* 8, 18 (1973).

[5]A. Barbaro-Galtieri *et al.*, Phys. Rev. Lett. 20, 349 (1968); H. J. Martin *et al.*, Phys. Lett. 22, 352 (1966); R. Barloutaud *et al.*, Phys. Lett. 26B, 674 (1968).

[6]E. H. Harvey *et al.*, Phys. Rev. Lett. 27, 885 (1971); P. Dalpiaz *et al.*, Phys. Lett. 42B, 377 (1972), and references given therein.

[7]D. M. Binnie *et al.*, Phys. Lett. 39B, 275 (1972).

[8]J. S. Danburg *et al.*, in *Experimental Meson Spectroscopy—1972*, edited by A. H. Rosenfeld and K. W. Lai (A.I.P., New York, 1972), p. 91; R. K. Kiang, University of Michigan, Ann Arbor, Ph.D. thesis, 1972 (unpublished).

[9]Particle Data Group, Phys. Lett. 39B, 1 (1972), or Rev. Mod. Phys. 45, S1 (1973).

[10]S. R. Borenstein *et al.*, Phys. Rev. D 5, 1559 (1972).

[11]The upper limit of 1.8 MeV of Binnie *et al.* (see Ref. 7) must be revised. The true width can be measured only

if the resolution is less than or approximately equal to it. Thus, an upper limit must be quoted using the variance of the χ^2 function to get the 95%-confidence-level upper limit, i.e., $2\sqrt{2}$ (No. degrees of freedom)$^{1/2}$ must be added, which is $2(2\times 8)^{1/2}=8$ (see, e.g., Ref. 9). This gives via Table I of Ref. 7, $\Gamma(\eta')<2.8$ MeV (95% C.L.).

[12] R. H. Dalitz, Philos. Mag. 44, 1068 (1953); E. Fabri, Nuovo Cimento 11, 479 (1954).

[13] V. I. Ogievetsky, W. Tybor, and A. N. Zaslavsky, Phys. Lett. 35B, 69 (1971); S. Giler *et al.*, Acta Phys. Pol. A37, 475 (1970).

[14] J. Klosinski, J. Rembielinski, and W. Tybor, Acta Phys. Pol. B1, 359 (1970); A. N. Zaslavsky, V. I. Ogievetsky, and W. Tybor, Yad. Fiz. 9, 852 (1969) [Sov. J. Nucl. Phys. 9, 498 (1969)], and private communications.

[15] G. R. Kalbfleisch *et al.*, Phys. Rev. Lett. 31, 333 (1973).

[16] D. L. Cheshire *et al.*, Phys. Rev. Lett. 28, 520 (1972).

[17] M. Aguilar-Benitez *et al.*, Phys. Rev. Lett. 25, 1635 (1970); and the third paper in Ref. 4; we note that a majority of their $M(953)$ events (if not all) are possibly $\eta'(958)$.

[18] B. Maglich *et al.*, Phys. Rev. Lett. 27, 1479 (1971); we note that H. Brody [*ibid.* 28, 1217 (1972); 28, 1497(E) (1972)] gives evidence that $\xi^0(953)$ is possibly the $\eta'(958)$.

[19] W. Kienzle *et al.*, Phys. Lett. 19, 438 (1965).

[20] The observation of $\delta^+(963)$ by J. Oostens *et al.* [Phys. Lett. 22, 708 (1966)] was contradicted by the data of M. A Abolins *et al.* (see Ref. 21).

[21] M. A. Abolins *et al.*, Phys. Rev. Lett. 25, 469 (1970).

[22] See reviews by B. Maglich [in *Proceedings of the Fifth International Conference on Elementary Particles, Lund, 1969,* edited by G. von Dardel (Berlingska Boktryckeriet, Lund, Sweden, 1970), p. 271], and by M. Derrick [in *High Energy Physics*, edited by K. T. Mahanthappa, W. D. Walker, and W. E. Britten (Colorado Associated Univ. Press, Boulder, 1970), p. 291].

[23] C. Defoix *et al.*, Nucl. Phys. B44, 125 (1972).

PHYSICAL REVIEW D VOLUME 8, NUMBER 11 1 DECEMBER 1973

Inclusive Reactions from π^+p at 4.1 GeV/c *

Douglas G. Fong, Anatole M. Shapiro, and Mildred Widgoff
Department of Physics, Brown University, Providence, Rhode Island 02912
(Received 27 February 1973)

At a π^+ beam momentum of 4.1 GeV/c, in reactions of the type $a+b\to c+X$, limiting fragmentation of the beam and target particles is observed where $ab\bar{c}$ is exotic, and is not observed for $ab\bar{c}$ not exotic. Single-particle distributions in several different variables have been studied for π^- and π^+ mesons. The two-particle distributions and correlation functions from the reaction $\pi^+ + p \to \pi^- + \pi^- + X$ are also presented.

I. INTRODUCTION

There has been much interest in inclusive reactions of the type $a+b\to c+X$, where X represents all other particles produced with c. There is considerable evidence that the distributions of certain kinematic quantities of particle c exhibit limiting behavior at very high energies,[1,2] and there are also theoretical arguments concerning just how high the energy has to be before "limiting" becomes discernible. Chan *et al.*[3] have argued from duality considerations that, if the combination $ab\bar{c}$ has quantum numbers that are exotic, the limiting may in fact show up at relatively low energies. In this paper, we present data from π^+p interactions at 4.1 GeV/c, corresponding to a center-of-mass energy of 2.92 GeV. For the inclusive reaction

$$\pi^+ + p \to \pi^- + X\,, \tag{1}$$

in which $ab\bar{c}$ is $\pi^+p\pi^+$, which has charge 3, baryon number 1, and is therefore exotic, it is of interest to see whether limiting behavior is observed at this low momentum. Results from previously published papers[4-6] at higher energies are shown for comparison and for indications of how limiting is approached. Data for

$$\pi^+ + p \to \pi^+ + X\,, \tag{2}$$

in which $ab\bar{c}$ is not exotic, are also shown for contrast. In addition, some information is presented concerning the two-body inclusive interaction

$$\pi^+ + p \to \pi^- + \pi^- + X\,. \tag{3}$$

The pictures in this experiment were taken with the Argonne-MURA 30-inch hydrogen bubble chamber. The sample considered here consisted of 22 000 events of all topologies, produced by 4.1-GeV/c π^+ mesons. About half of the sample was measured on the MIT PEPR (precision encoding and pattern recognition) system, and the rest on semiautomatic precision machines. TVGP and SQUAW were used for geometrical reconstruc-